Article

Perception of viral infections and initiation of antiviral defence in rice

https://doi.org/10.1038/s41586-025-08706-8

Received: 23 January 2024

Accepted: 27 January 2025

Published online: 12 March 2025

Open access

Check for updates

Yu Huang[1,11,12], Jialin Yang[2,3,12], Xi Sun[1,3,12], Jiahao Li[1,3], Xiaoqiang Cao[4,5], Shengze Yao[1], Yanhong Han[3], Changtian Chen[3], Linlin Du[6], Shuo Li[6], Yinghua Ji[6], Tong Zhou[6], He Wang[7], Jia-jia Han[8], Wenming Wang[7], Chunhong Wei[1], Qi Xie[4,5,9], Zhirui Yang[10] ✉ & Yi Li[1,3] ✉

Crop production faces persistent threats from insect-vector-borne viral diseases[1,2]. Recent advancements have revealed the intricate immune mechanisms that plants deploy against viral pathogens[3–8]. However, the molecular mechanisms through which plant hosts recognize viral infections and initiate antiviral defence at disease onset have not been elucidated. Here, through the natural infection of rice by inoculation with insect vectors carrying the natural forms of viruses, we show that viral coat proteins are perceived by the RING1–IBR–RING2-type ubiquitin ligase (RBRL), initiating the first step of the natural antiviral response in rice. RBRL subsequently targets an adaptor protein of the transcriptional repression complex of the jasmonate pathway, NOVEL INTERACTOR OF JAZ 3 (NINJA3), for degradation through the ubiquitination system, inducing jasmonate signalling and activating downstream antiviral defence. We further show that this phenomenon is a universal molecular mechanism used by rice plants to perceive viral infections and initiate antiviral signalling cascades. This approach is important not only for obtaining a deeper understanding of virus–host interactions but also for further disease resistance breeding.

Rice (*Oryza sativa*) is a staple food for approximately half the global population, and its production is facing a serious threat of numerous insect-vector-transmitted diseases, such as rice stripe disease, caused by rice stripe virus (RSV)[9–12].

RSV, a member of the *Tenuivirus* genus, is transmitted by the small brown planthopper (*Laodelphax striatellus* Fallén)[13]. The vector insects use their needle-like piercing mouthparts to deliver virions into host cells while sucking plant nutrients[14]. This process differs from that used by animal viruses, which enter host cells through specific receptors[15]. To date, no receptor for plant viruses has been identified[16].

We have shown that the RSV coat protein (CP) is an effector that triggers the accumulation of jasmonic acid (JA) and subsequently upregulates the transcription of the antiviral RNA silencing core factor *ARGONAUTE 18* (*AGO18*) through the JA-responsive MYB transcription factor (JAMYB)[17]. AGO18 functions as a decoy, sequestering microRNA168 (miR168) and miR528 away from AGO1[18–20]. This action leads to the release of target genes *AGO1* and *L-ascorbate oxidase* (*AO*), thereby strengthening the antiviral defence[18,19]. However, there is limited information concerning the intricate mechanism through which rice perceives RSV infection and orchestrates this signalling cascade to activate the antiviral response[17].

JA and its derivatives are present throughout the plant kingdom[21] and have pivotal roles in plant defence against necrotrophic pathogens, chewing insects and mechanical damage[22]. The JA pathway functions in a classical relief-of-repression model. In the absence of JA-Ile, jasmonate-ZIM domain (JAZ) proteins recruit TOPLESS (TPL) and TOPLESS-RELATED (TPR) corepressors through NINJA proteins, ultimately suppressing the transcription of JA-responsive genes[23,24]. When JA-Ile is synthesized, interactions between JAZ repressors and the F-box protein CORONATINE INSENSITIVE 1 (COI1) trigger JAZ degradation through the 26S proteasome, liberating JA-responsive transcription factors to modulate gene transcription[17,25–27]. Although considerable efforts have been made to elucidate the biosynthesis and transduction of jasmonate signals[28–30], study of the turnover of NINJA proteins is lacking.

Ubiquitination regulates eukaryotic cellular processes, such as signal transduction, immune responses and apoptosis[31]. Ubiquitination is coordinated by ubiquitin-activating enzymes (E1s), ubiquitin-conjugating enzymes (E2s) and ubiquitin ligases (E3s)[32]. E3 ligases, including really interesting new genes (RINGs; topologically similar U-box E3s), homologous to the E6-AP C terminus (HECTs) and the more recently recognized RING1–IBR–RING2 (RBR)-type E3 ligases, are closely associated with viral infection[33–36]. In mammals, RBR-type E3 ligases exhibit a RING/HECT hybrid-like function; they bind to E2s through RING1 and catalyse ubiquitin transfer through the formation of an obligate thioester-linked ubiquitin (Ub) with the conserved cysteine residue in RING2[37,38]. Despite their evolutionary persistence,

[1]State Key Laboratory of Gene Function and Modulation Research, School of Life Sciences, Peking University, Beijing, P. R. China. [2]Academy for Advanced Interdisciplinary Studies, Peking University, Beijing, P. R. China. [3]State Key Laboratory of Agricultural and Forestry Biosecurity, Vector-borne Virus Research Center, Institute of Plant Virology, Fujian Agriculture and Forestry University, Fuzhou, P. R. China. [4]Institute of Genetics and Developmental Biology, The Innovative Academy of Seed Design, Chinese Academy of Sciences, Beijing, P. R. China. [5]University of Chinese Academy of Sciences, Beijing, P. R. China. [6]Institute of Plant Protection, Jiangsu Academy of Agricultural Sciences, Nanjing, P. R. China. [7]State Key Laboratory of Crop Gene Exploration and Utilization in Southwest China, Sichuan Agricultural University, Chengdu, P. R. China. [8]Institute of Biodiversity, School of Ecology and Environmental Science Yunnan University, Kunming, P. R. China. [9]National Center of Technology Innovation for Maize, State Key Laboratory of Crop Germplasm Innovation and Molecular Breeding, Syngenta Group China, Beijing, P. R. China. [10]State Key Laboratory of Plant Environmental Resilience, College of Biological Science, China Agricultural University, Beijing, P. R. China. [11]Present address: Sichuan Institute of Edible Fungi, Sichuan Academy of Agricultural Sciences, Chengdu, P. R. China. [12]These authors contributed equally: Yu Huang, Jialin Yang, Xi Sun. ✉e-mail: rynn_yang@cau.edu.cn; liyi@pku.edu.cn

the regulatory and biological roles of plant RBR-type E3 ligases have largely not been explored[39–41].

Here we show that rice perceives RSV infection through the RBR-type E3 ligase RBRL, which then orchestrates the ubiquitination-mediated degradation of NINJA3, a transcriptional repressor. This process initiates JA signalling followed by RNA-silencing-mediated antiviral defence, offering insights into the intricate antiviral responses of rice.

OsRBRL perceives RSV infection

To better understand how RSV CP triggers JA signalling-coupled antiviral defence, we analysed the subcellular localization of RSV CP in RSV-infected wild-type rice NPB (*O. sativa* subsp. *japonica* cv. Nipponbare) and *CP*-overexpressing (*CP*-OE) plants. Notably, RSV CP was partially localized in the nucleus, suggesting that it may function as a signalling factor for viral perception (Fig. 1a,b; immunoblot source data are provided in Supplementary Fig. 1). We performed immunoprecipitation–mass spectrometry (IP–MS) assays using the nuclear fractions shown in Fig. 1b to identify proteins interacting with CP. Among the CP-interacting proteins, an RBR-type ubiquitin ligase, named OsRBRL, was found in the prey lists from RSV-infected NPB and *CP*-OE samples (Extended Data Fig. 1a and Supplementary Table 1). Phylogenetic analysis of OsRBRL identified an OsRBRL-like protein in the same subclade as RBRL. A conserved motif analysis revealed that RBRL and RBRL-like proteins possess the classic RING1–IBR–RING2 domains (Extended Data Fig. 1b,c).

The interaction between CP and OsRBRL was further validated by co-immunoprecipitation (co-IP), luciferase complementation imaging (LCI) and pull-down assays (Fig. 1c,d and Extended Data Fig. 2a–c). The LCI assays showed that CP did not interact with OsRBRL-like (Fig. 1d). Microscale thermophoresis (MST) assays further showed a strong binding affinity between CP and RBRL with a dissociation constant (K_d) of 5.28 nM (Extended Data Fig. 2d). Moreover, LCI assays showed that CP interacts with RBRL through the C-terminal Ariadne (Ari) domain, N-terminal domain (NTD) and RBR domain (Extended Data Fig. 2e,f).

Importantly, we observed that the expression of *OsRBRL* mRNA and OsRBRL protein was induced by RSV infection and *CP* overexpression (Fig. 1e–h and Extended Data Fig. 1d). However, transcriptome deep sequencing (RNA-sequencing, RNA-seq) data indicated that the expression levels of *OsRBRL-like* did not significantly change after RSV infection (Extended Data Fig. 1d). Moreover, OsRBRL-like did not interact with CP (Fig. 1d); we therefore focused on *OsRBRL* for further study.

OsRBRL initiates the JA signalling pathway

To further investigate the function of OsRBRL, we obtained the *rbrl*-knockout mutant and *RBRL*-overexpressing (*RBRL*-OE) rice lines (Extended Data Fig. 2g,l). The transcript levels of *CM-LOX1*, *CM-LOX2*, *OsAOS2* and *OsJMT1* (involved in JA biosynthesis), as well as those of *OsCOI1A*, *OsCOI1B*, *OsCOI2*, *OsJAMYB*, *OsAGO18* and multiple *OsJAZ* genes (involved in JA signalling), were downregulated in the *rbrl* mutants but upregulated in the *RBRL*-OE plants compared with the NPB plants (Fig. 1i). Immunoblotting results confirmed these findings, showing lower protein levels of CM-LOX2 and AOS2 in *rbrl* lines and higher levels in *RBRL*-OE lines than in NPB plants (Fig. 1j). The JA levels were significantly decreased in the *rbrl* mutant but substantially increased in the *RBRL*-OE plants (Fig. 1k,l). In particular, after RSV infection, the JA content was higher in *RBRL*-OE rice plants and lower in *rbrl* mutants than in NPB plants (Fig. 1k,l), indicating that RBRL contributes to RSV-induced JA accumulation. To further elucidate the broad role of OsRBRL in regulating the response of rice plants to viral infection, we performed RNA-seq and comparative transcriptome analysis in NPB, *rbrl* and *RBRL*-OE plants with or without RSV infection. We identified numerous potential RBRL-regulated differentially expressed genes (DEGs). Gene Ontology (GO) analysis revealed high enrichments of genes related to defence, JA signalling and reactive oxygen species (ROS) pathway (Extended Data Fig. 2g–p and Supplementary Table 2).

Taken together, these results indicated that *OsRBRL* might act as a sensor of viral CP and exert a positive regulatory influence on JA biosynthesis and JA signalling.

RBRL is required in antiviral defence

Subsequently, we investigated whether the interaction between RSV CP and OsRBRL was correlated with CP-mediated rice antiviral defence. We performed natural infection of rice lines with RSV-carrying small brown planthoppers and compared disease symptoms in NPB, *rbrl*-mutant and *RBRL*-OE lines (Fig. 2a,b). Notably, compared with the NPB plants, the *rbrl*-mutant plants exhibited more pronounced stunting after RSV infection, whereas the *RBRL*-OE plants displayed less stunting (Fig. 2a). The disease symptoms were subsequently categorized based on their severity on leaves (Extended Data Fig. 3a). Compared with the NPB plants, *rbrl* plants displayed fewer symptomless (grade N) leaves and more severe symptoms (grade III). Conversely, *RBRL*-OE plants showed more symptomless (grade N) leaves, and fewer typical (grade II) and severe symptoms (grade III) (Fig. 2b and Supplementary Table 3). Consistent with these phenotypic observations, the accumulation of RSV CP and viral RNAs was significantly increased in the *rbrl* mutants and substantially decreased in the *RBRL*-OE lines (Fig. 2c,d).

A previous study showed that RSV CP activates the JA signalling pathway, thereby inducing the expression of *OsAGO18*[17]. *CP*-OE plants exhibited higher OsAGO18 protein levels compared with NPB plants, and the expression of *OsAGO18* and *CP* was correlated[18]. Thus, the accumulation of OsAGO18 serves as a marker for the rice antiviral defence. Notably, RSV-infected *rbrl* plants accumulated more CP but less OsAGO18 compared with RSV-infected NPB plants (Fig. 2c). Conversely, RSV-infected *RBRL*-OE plants showed lower CP and higher OsAGO18 levels (Fig. 2c). These results strongly suggest that OsRBRL bridges RSV CP and the JA-signalling-coupled antiviral RNA interference (RNAi) pathway.

To further confirm that the perception of CP by OsRBRL is essential for activating downstream antiviral signalling, we overexpressed *CP* in the *rbrl*-mutant background, generating two lines: *CP*-OE/*rbrl* 1 and *CP*-OE/*rbrl* 2. These *CP*-OE/*rbrl* lines displayed moderate resistance compared with NPB plants, whereas their antiviral responses were weakened compared with those of the *CP*-OE plants[17] (Fig. 2e,f and Supplementary Table 3). Furthermore, the levels of viral RNA and accumulated CP in the *CP*-OE/*rbrl* lines were between those in the NPB and *CP*-OE plants[17] (Fig. 2g,h). Notably, the accumulation of OsAGO18 also followed this pattern (Fig. 2h). As RSV CP accumulated significantly higher in RSV-infected NPB plants than in *CP*-OE plants (Extended Data Fig. 3b), we propose that a low dose of CP is sufficient to be sensed by RBRL for initiating the JA–AGO18 antiviral signalling. A comparison of the *CP*-OE/*rbrl* lines with the *rbrl*-mutant lines revealed that overexpression of *CP* partially rescued the sensitive phenotypes of the *rbrl*-mutant plants after RSV infection, suggesting that natural antiviral signalling is initiated in rice plants not entirely, but mainly through OsRBRL.

A previous study showed that the expression of *OsAGO18* is regulated by JAMYB and inhibited by JAZ6[17]. To determine whether OsRBRL affects the activation of antiviral immunity by regulating *OsAGO18* transcription, we co-expressed *35S::YFP-JAMYB*, *35S::MYC-JAZ6*, *AGO18pro::LUC* and *35S::HA-RBRL* in tobacco leaves or rice protoplasts (a list of the primers used to construct these vectors is provided in Supplementary Table 5). Consistent with previous reports, JAZ6 inhibited the transcriptional activity of the *OsAGO18* promoter[17]. However, increasing the expression of *35S::HA-RBRL* significantly derepressed *AGO18pro::LUC*, and the activation of *AGO18pro::LUC* was specifically rescued by the co-expression of *35S::HA-RBRL* but not *35S::HA-RBRL-like* (Extended Data Fig. 3c–e).

Moreover, co-IP assays using the nuclear fraction of mock-inoculated and RSV-infected *RBRL*-OE samples demonstrated that CP interacts

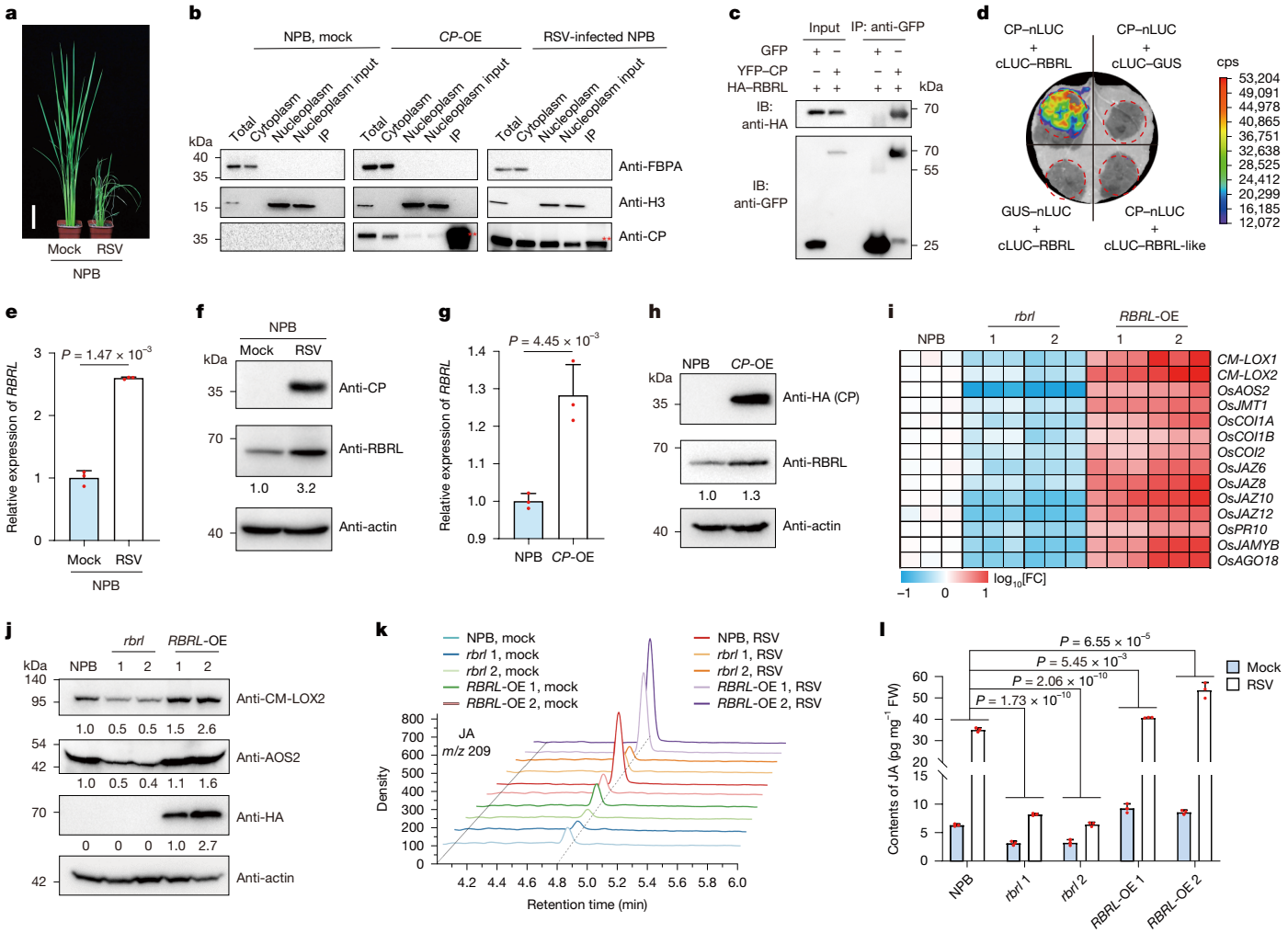

Fig. 1 | OsRBRL perceives CP and activates JA biosynthesis and signalling. **a**, Photographs of mock-inoculated and RSV-infected wild-type NPB rice plants. The photographs were captured at 4 weeks post-infection (w.p.i.). Scale bar, 10 cm. **b**, IP–MS assays conducted with the nuclear fraction of mock-inoculated NPB plants, *CP*-OE plants and RSV-infected NPB plants. FBPA was used as a cytoplasmic marker, and histone H3 as a nuclear marker. **c**, Co-IP assays illustrating the interaction between RSV CP and OsRBRL in *N. benthamiana* leaves through YFP–CP and HA–RBRL. GFP was used as a negative control. IB, immunoblotting. The analyses in **b** and **c** were repeated two to three times with similar results. **d**, LCI assays demonstrating the interaction between RSV CP and OsRBRL. cLUC–GUS and GUS–nLUC were used as negative controls. cps, signal counts per second. **e**,**g**,**i**, RT–qPCR results showing the expression levels of *OsRBRL* (**e** and **g**) or genes related to JA synthesis and signalling (**i**) in the indicated plants. **f**,**h**,**j**, Immunoblotting analysis of the indicated protein levels in the indicated plants. Actin was used as a sample processing control. The analyses were repeated three to five times with similar results. **k**,**l**, LC–MS analysis (**k**) and quantification (**l**) of the JA concentrations in the NPB, *rbrl* and *RBRL*-OE plants with or without RSV infection. Rice plants were collected at 3 w.p.i. Statistical analysis was performed using two-sided Student's *t*-tests (**e** and **g**) and two-way analysis of variance (ANOVA) (**l**), the *P* values in **l** indicate the interactions between genotype and treatment. All *P* values are shown in the figure. Data are mean ± s.d. $n = 3$ independent biological samples.

with RBRL in the nuclear fraction (Extended Data Fig. 4a). RSV CP and OsRBRL were colocalized in the nucleoplasm and cytoplasm of the rice protoplasts (Extended Data Fig. 4b). Transient expression of OsRBRL containing a nuclear export signal (NES) at the N terminus (OsRBRL(NES)) in rice protoplasts showed higher virus accumulation compared with transient expression of OsRBRL (Extended Data Fig. 4c,d). These data suggest that OsRBRL mediates antiviral defence in the nucleus.

Taken together, these results suggest that the CP-induced rice antiviral defence requires OsRBRL to relieve the repression of JA signalling and therefore promote the expression of JA-responsive genes and *OsAGO18*.

CP enhances OsRBRL's E3 ligase activity

To elucidate the molecular function of RBRL, we performed self-ubiquitination assays using the plant ubiquitination cascade reconstituted in bacteria[42]. The results confirmed that OsRBRL possesses E3 ligase activity (Fig. 3a). Sequence analysis of the RBRL protein showed that OsRBRL is a member of the Ariadne subfamily of RBR-type E3 ligases (Fig. 3b and Extended Data Fig. 1b). In humans, these ligases typically undergo autoinhibition. Removing the Ariadne domain activates the human homologue of Ariadne (HHARI)[37]. HHARI and the mammalian homologue of ari-2 (TRIAD) are activated after binding to neddylated Cullin–RING ligase complexes[39,43]. However, research on the mechanism underlying their activation is limited[39]. We observed that removing the NTD and Ariadne domains of OsRBRL resulted in instability of the OsRBRL RBR domain when expressed independently in plant cells (Fig. 3c). Moreover, self-ubiquitination assays in the bacterial system revealed that the conserved cysteine residue (Cys305) in the RING2 domain is essential for the activity of RBRL, and RSV CP increased the activity of RBRL (Fig. 3d,e). Semi-in vivo degradation assays revealed that, compared with the control, RSV CP promoted the degradation of RBRL (Fig. 3f). These results indicate

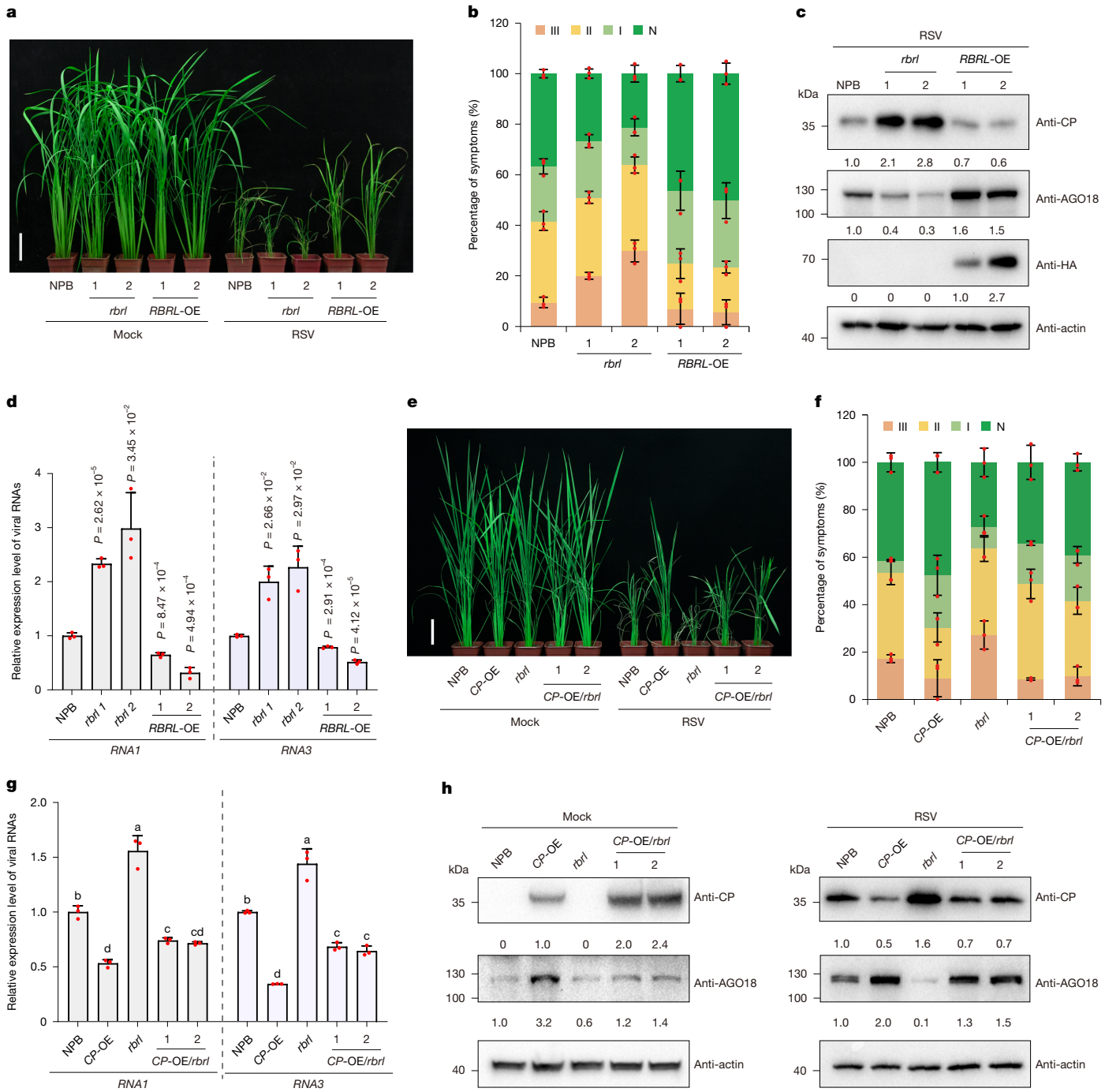

Fig. 2 | The CP-induced natural antiviral defence requires RBRL. a, Images of mock-inoculated or RSV-infected NPB, *rbrl* and *RBRL*-OE plants. Scale bar, 10 cm. **b**, The percentages of RSV-infected NPB, *rbrl* and *RBRL*-OE plants with various disease symptom grades. Data are mean ± s.d. $n = 3$ independent biological experiments. **c**, Immunoblotting analysis of the RSV CP and AGO18 levels in the specified plants. OsRBRL expressed in *RBRL*-OE lines 1 and 2 was labelled with a 1× HA tag at the N terminus. Actin was used as a sample processing control. **d**, RT–qPCR analysis of RSV RNA accumulation in the specified plants. Statistical analysis was performed using two-sided Student's *t*-tests, and all *P* values are shown in the figure. Data are mean ± s.d. $n = 3$ independent biological samples. **e**, Images showing mock-inoculated or RSV-infected NPB, *CP*-OE, *rbrl* and *CP*-OE/*rbrl* plants. Scale bar, 10 cm. **f**, The percentages of RSV-infected NPB, *CP*-OE, *rbrl* and *CP*-OE/*rbrl* plants with various disease symptom grades. Data are mean ± s.d. $n = 3$ independent biological experiments. **g**, RT–qPCR analysis of RSV RNA accumulation in the specified plants. Statistical analysis was performed using one-way ANOVA with Tukey's multiple-comparison test (different letters represent significantly different groups; $P < 0.05$). Data are mean ± s.d. $n = 3$ independent biological samples. **h**, Immunoblotting analysis of the RSV CP and AGO18 levels in the specified plants. All of the mock-inoculated rice plants were 6 weeks old and all of the RSV-infected plants were collected at 4 w.p.i. Actin was used as a sample processing control. All of the experiments were repeated two to four times with similar results.

that the natural state of RBRL is partially autoinhibited, as reported for homologues, and that the CP–RBRL interaction could activate the E3 ligase activity of RBRL.

Although E3 ligase usually interacts with and targets viral proteins for degradation, CP is not ubiquitinated in RSV-infected NPB or *RBRL*-OE rice plants, nor in degradation assays performed in bacterial systems or tobacco leaves (Extended Data Fig. 4e–g), suggesting that CP is not the substrate of RBRL. The CP–RBRL interaction may promote the degradation of a substrate to trigger downstream antiviral defence.

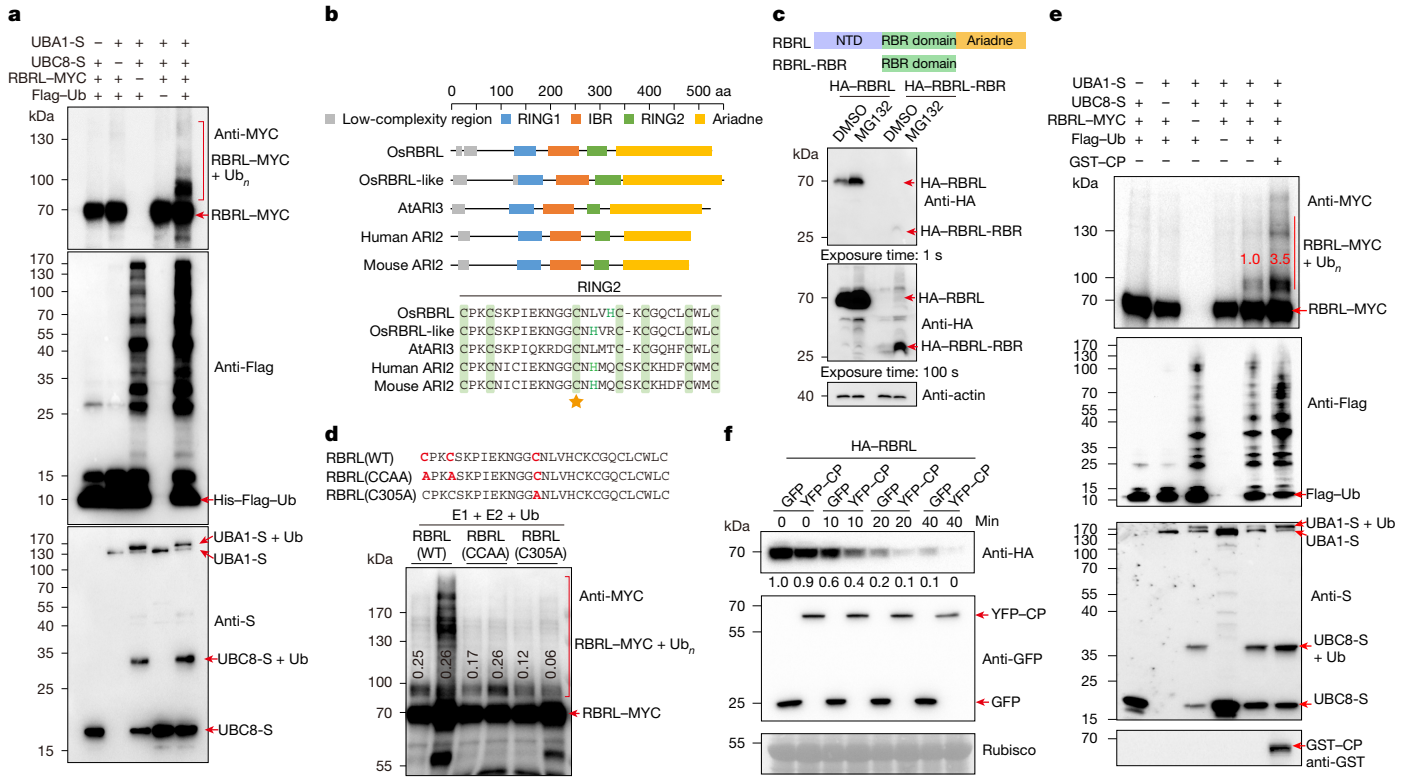

Fig. 3 | RBRL acts as an active E3 ligase and CP enhances its activity. **a**, Autoubiquitination analysis of OsRBRL. The bacterial lysates from *Escherichia coli* strains expressing UBA1-S (E1), UBC8-S (E2), Flag–Ub and RBRL–MYC or from strains lacking one of these components were analysed by immunoblotting with anti-MYC (top), anti-Flag (middle) or anti-S (bottom) antibodies. **b**, The domain compositions of OsRBRL, OsRBRL-like, *Arabidopsis thaliana* ARI3 (AtARI3), human ARI2 and mouse ARI2. An asterisk indicates the reported active site of human ARI2. **c**, The effect of MG132 on the stability of the full-length OsRBRL and the RBR domain of OsRBRL. Actin was used as a sample processing control. **d**, Autoubiquitination of OsRBRL and its corresponding point mutants. The RBRL–MYC + Ub$_n$/RBRL–MYC ratios are listed. **e**, CP enhanced the ubiquitin ligase activity of OsRBRL. The bacterial lysates from *E. coli* strains expressing UBA1-S, UBC8-S, Flag–Ub, RBRL–MYC and GST–CP or from strains lacking one of these components were analysed by immunoblotting using anti-MYC (row 1), anti-Flag (row 2), anti-S (row 3) and anti-GST (row 4) antibodies. **f**, Time-course analysis of CP-promoted OsRBRL self-degradation. The OsRBRL degradation assay was performed by mixing cell extracts from separately infiltrated GFP, YFP–CP and HA–RBRL samples, and GFP was used as a negative control. Ponceau S staining (bottom) of the Rubisco protein is shown as a loading control. All of the experiments were repeated two to four times with similar results.

OsRBRL targets NINJA3 for degradation

To identify the mechanisms underlying OsRBRL-mediated modulation of the JA signalling pathway, we conducted IP–MS assays focusing on potential ubiquitination substrates. The results revealed that OsNINJA3, an adaptor protein that links JAZ proteins to their corepressor TPL/TPR, is a potential substrate (Extended Data Fig. 5a,b and Supplementary Table 4). Phylogenetic analysis revealed that rice NINJA1/2/3 proteins belong to the same subclade as most NINJA proteins in monocotyledonous plants (Extended Data Fig. 5c). Notably, this subclade is closely related to the ABA INSENSITIVE FIVE BINDING PROTEINS (AFPs) found in dicot plants (Extended Data Fig. 5c). Moreover, rice NINJA4 and maize NINJA7/8 proteins fall within the same subclade as the NINJA proteins from *Arabidopsis* and tobacco (Extended Data Fig. 5c). Conserved motif analysis showed that NINJA proteins mainly contain four conserved motifs: EAR, NINJA-B, ZBD core and ZBD NTE motifs (Extended Data Fig. 5c). We subsequently examined the interactions between OsRBRL and OsNINJA proteins through yeast two-hybrid (Y2H), LCI and pull-down assays. The results indicated that OsRBRL interacted with OsNINJA1/2/3 but not OsNINJA4 (Fig. 4a–c and Extended Data Fig. 5d–h). The full-length OsNINJA1/2/3 proteins interacted mainly with the NTD and RBR domains of RBRL, while the full-length RBRL protein interacted with the ZBD NTE motif- and NINJA-B motif-containing domains of the NINJA3 protein (Extended Data Fig. 5f–h). Notably, RSV-infected rice plants showed significantly decreased protein levels of OsNINJA3, and several higher-molecular-mass proteins were detected in these plants through the anti-NINJA3 antibody (Fig. 4d). These results suggested that OsNINJA3 might be a substrate of OsRBRL and could be degraded after RSV infection.

To test our hypothesis, we conducted protein degradation assays in tobacco leaves. Increasing the expression of HA–RBRL rather than HA–RBRL-like, the protein level of YFP–NINJA3 but not that of YFP–NINJA4 decreased (Extended Data Fig. 6a). Furthermore, we validated these findings using a semi-in vivo system. In the presence of the HA–RBRL protein, the protein level of YFP–NINJA3, but not that of YFP–NINJA4, was significantly decreased (Fig. 4e,f). We further showed that the degradation of YFP–NINJA3 was significantly attenuated by MG132, suggesting that the OsRBRL-mediated degradation of OsNINJA3 occurs through the 26S proteasome (Extended Data Fig. 6b). Moreover, increasing the level of RSV CP promoted the proteolysis of NINJA3 but not that of NINJA4 by activating RBRL (Extended Data Fig. 6c).

As the 26S proteasome primarily recognizes ubiquitinated proteins and a potential ubiquitinated form of OsNINJA3 was detected in RSV-infected rice (Fig. 4d), we examined whether OsRBRL directly ubiquitinates OsNINJA3. Ubiquitination assay in the bacterial system[42] showed that ubiquitination of OsNINJA3 occurred only in the presence of E1, E2, OsRBRL and ubiquitin (Fig. 4g). Importantly, increased ubiquitination of OsNINJA3 was observed when RSV CP was added to the system (Extended Data Fig. 6d).

To confirm the above results, we co-expressed *NINJA3-GFP* with *HA-RBRL* or empty vector (EV) in NPB protoplasts. The NINJA3–GFP signal was substantially weaker in cells co-expressing RBRL than in

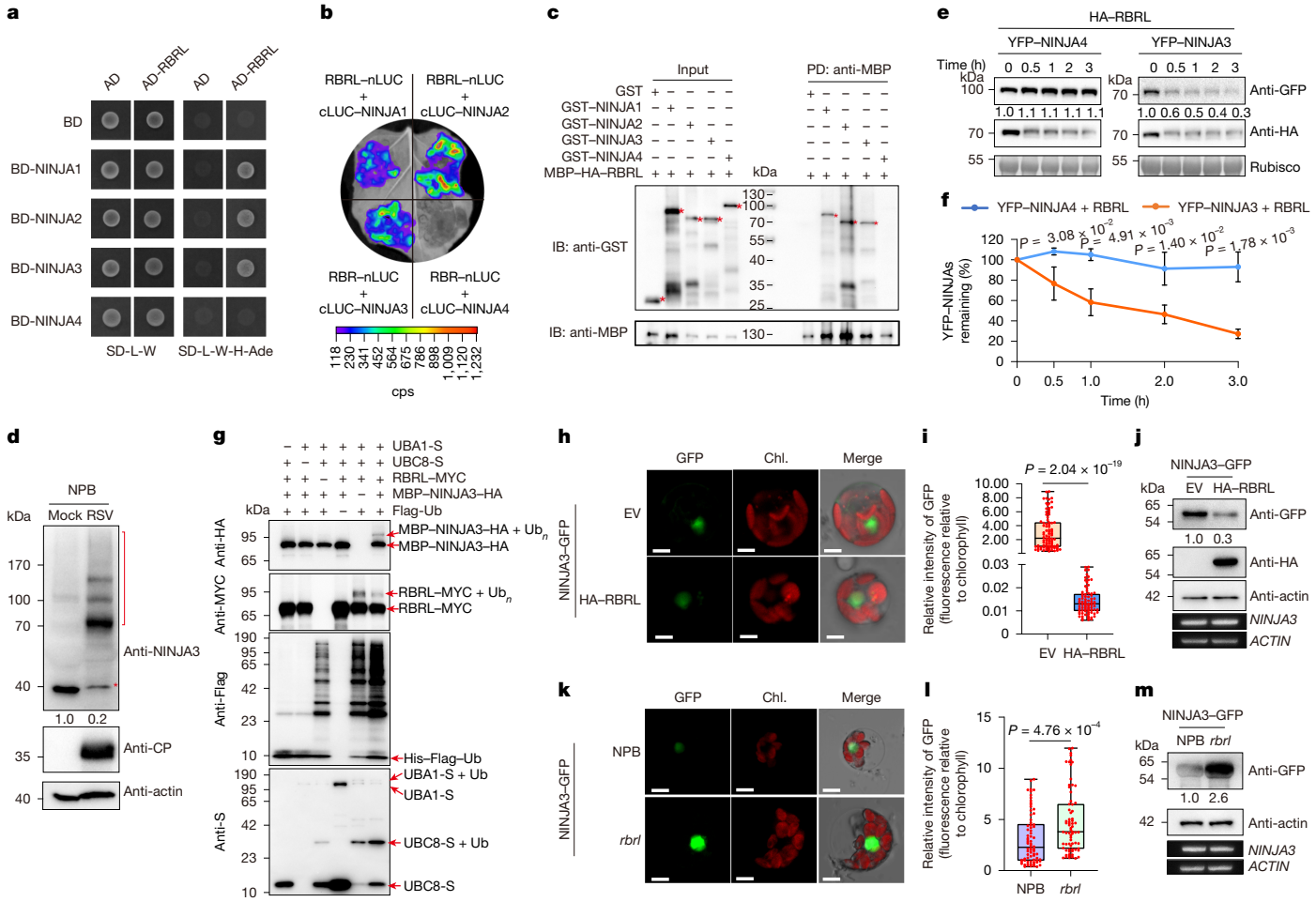

Fig. 4 | RBRL targets NINJA3 for degradation. **a**–**c**, Y2H (**a**), LCI (**b**) and pull-down (PD) (**c**) assays analysing the interactions between OsNINJAs and OsRBRL. **d**, Immunoblotting of OsNINJA3 in mock-inoculated or RSV-infected NPB plants (indicated by the asterisk). The red line denotes higher-molecular-mass derivatives of OsNINJA3. Actin was used as a processing control. **e**, Time-course analysis of RBRL-promoted NINJA3 degradation. YFP–NINJA4 was used as a negative control. Ponceau S staining of the Rubisco proteins was used as a sample processing control. **f**, The intensities of the bands shown in **e** were quantified using ImageJ. Relative values were calculated by comparison with the values at 0 h (set to 1.0). Data are mean ± s.d. $n = 3$ independent biological samples. **g**, Ubiquitination of NINJA3 by RBRL. Bacterial lysates from the indicated *E. coli* strains were analysed by immunoblotting. **h**–**m**, The NINJA3–GFP signal was affected by OsRBRL in rice protoplasts. Fluorescence of GFP–NINJA3 in NPB rice protoplasts, NPB rice protoplasts transformed with empty vector or *35S::HA-RBRL* overexpression vector (**h**–**j**) and *rbrl* rice protoplasts (**k**–**m**) was analysed using confocal microscopy (**h**,**k**). Scale bars, 5 μm (**h** and **k**). **i**,**l**, The NINJA3–GFP signal was quantified and normalized to the chlorophyll fluorescence. $n = 81$ and 87 cells (**i**) and 74 and 71 cells (**l**) over two independent biological experiments. For the box plots in **i** and **l**, the centre line shows the median, the box limits show the upper and lower quartiles, the whiskers show the minimum to the maximum, and the points show individual values. **j**,**m**, Immunoblotting analysis of the NINJA3–GFP levels in **h** and **k**. Actin was used as a loading control (middle). *NINJA3* and *ACTIN* mRNA levels were analysed using RT–PCR (bottom). For **f**, **i** and **l**, statistical analysis was performed using two-sided Student's *t*-tests; all *P* values are shown in the figures. All of the experiments were repeated two to four times with similar results.

cells expressing the EV (Fig. 4h,i). Consistently, immunoblotting indicated that HA–RBRL significantly reduced NINJA3–GFP levels while the *NINJA3* mRNA level was equivalent across various co-transformation conditions (Fig. 4j). We extended this analysis using rice protoplasts extracted from the NPB and *rbrl* mutants. The signal intensity of NINJA3–GFP was substantially higher in protoplasts from the *rbrl* mutants than in those from the NPB plants (Fig. 4k,l). Notably, the protein levels of NINJA3–GFP were consistent with the fluorescence results (Fig. 4m). Importantly, the protein levels of OsNINJA3 were lower in the *RBRL*-OE lines and greater in the *rbrl*-mutant lines compared with those in the NPB plants (Extended Data Fig. 6e). Furthermore, with RSV infection, higher-molecular-mass proteins (ubiquitinated OsNINJA3) accumulated in the NPB and *RBRL*-OE lines but not in the *rbrl*-mutant plants (Extended Data Fig. 6e). This is possibly due to the CP-enhanced RBRL-mediated ubiquitination of NINJA3 and the irregular proteasome assembly in RSV-infected plants (Extended Data Fig. 6d,f).

Collectively, these results provided strong evidence showing that, after RSV infection, CP activates the E3 ligase activity of OsRBRL to mediate the ubiquitination and subsequent degradation of OsNINJA3 through the ubiquitination system, therefore inducing jasmonate signalling. These findings revealed a mechanism for relieving plant RBR-type E3 ligase autoinhibition and the turnover mechanism of OsNINJA3.

NINJA3 suppresses antiviral JA signalling

Although AFP2 and AFP3 have been shown to not interact with JAZ1 in *Arabidopsis*[24], the *afp2* mutant presented phenotypes similar to those of the *Arabidopsis jaz-D* (decuple *JAZ* mutant) mutant[44], indicating that AFPs in dicotyledonous plants may be involved in the regulation of JA signalling. Rice NINJA1 interacts with most OsJAZs and inhibits JA signalling by recruiting of OsTPR1[45], suggesting that NINJAs or AFPs of monocotyledonous crop species may have evolved different functions

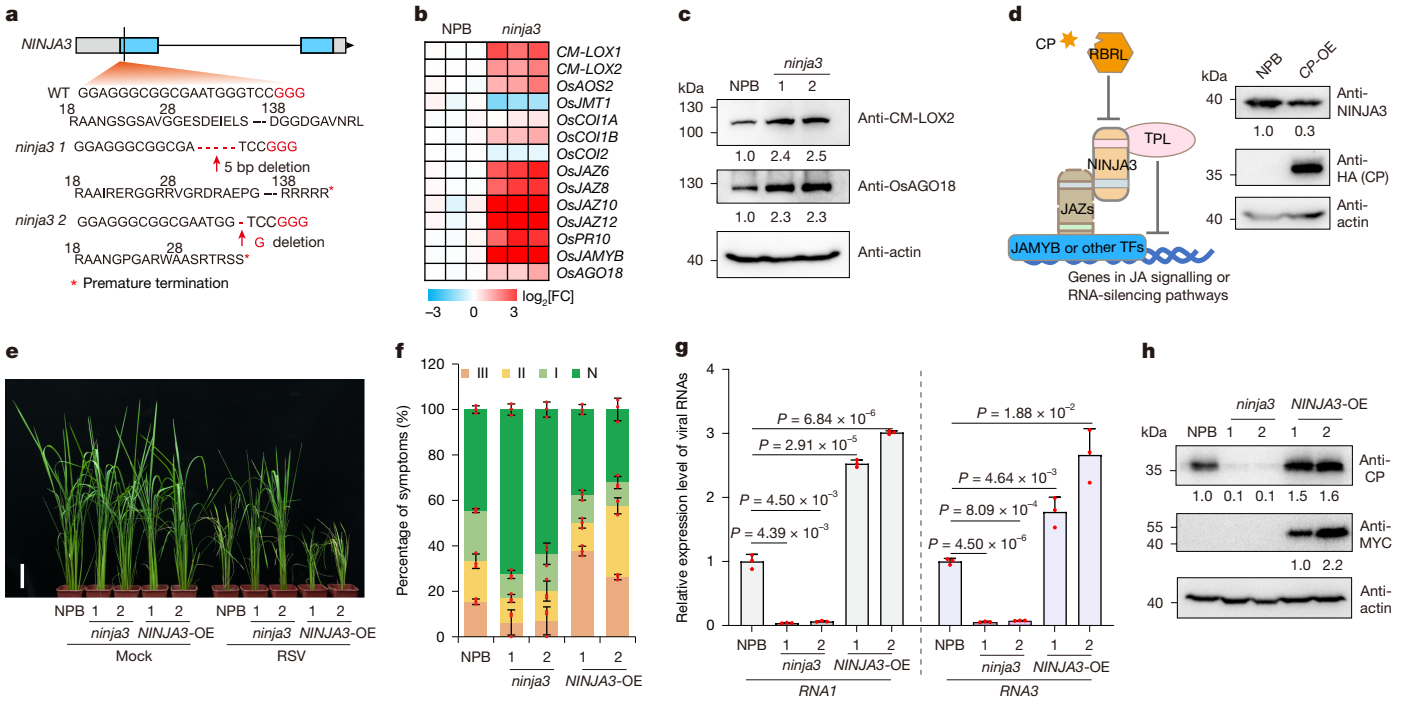

Fig. 5 | NINJA3 negatively regulates JA signalling and compromises rice antiviral defence. a, Construction of *ninja3*-knockout (CRISPR–Cas9) lines. The sgRNA sequence that specifically targets *OsNINJA3* is indicated, and the PAM is highlighted in red. The deletions in the sgRNA target sites in *ninja3* lines led to premature termination of the translation of *OsNINJA3*. **b**, RNA-seq analysis of the expression levels of genes related to JA synthesis and signalling in the NPB and *ninja3* rice lines. **c**, Immunoblotting analysis of the indicated protein levels in the NPB and *ninja3* rice lines. **d**, Schematic of RBRL and NINJA3 in regulating gene expression and immunoblot analysis of the OsNINJA3 levels in the indicated plants. **e**, Photographs of mock-inoculated or RSV-infected NPB, *ninja3* and *NINJA3*-OE plants. Scale bar, 10 cm. **f**, The percentages of RSV-infected NPB, *ninja3* and *NINJA3*-OE plants with different disease symptom grades. Data are mean ± s.d. $n = 3$ independent biological experiments. **g**, RT–qPCR analysis of RSV RNA accumulation in the indicated plants. Statistical analysis was performed using two-sided Student's *t*-tests; all *P* values are shown in the figure. Data are mean ± s.d. $n = 3$ independent biological samples. **h**, Immunoblotting analysis of the RSV CP levels in the indicated plants. OsNINJA3 expressed in *NINJA3*-OE lines 1 and 2 was labelled with a 3× MYC tag at the N terminus. Actin in **c**, **d** and **h** was used as a sample processing control. All of the rice plants were collected at 4 w.p.i. All of the experiments were repeated two to four times with similar results. TFs, transcription factors.

in regulating plant growth and stress responses. To examine the role of OsNINJA3 in antiviral defence, we knocked out *OsNINJA3* to generate *ninja3*-mutant lines (Fig. 5a) and performed RNA-seq analysis of NPB and *ninja3* mutants with or without RSV infection. We identified 9,942 DEGs between NPB and *ninja3* mutants under mock-inoculated and RSV-infected conditions (Extended Data Fig. 7a–c). GO analysis revealed that these DEGs were enriched in biological processes associated with cell division, ROS metabolic processes, response to JA stimulus, RNAi and abscisic acid signalling pathways (Extended Data Fig. 7d). Consistently, the absence of *NINJA3* led to the activation of JA biosynthesis- and signalling-responsive genes, including the rice antiviral defence marker gene *OsAGO18* (Fig. 5b,c).

We further demonstrated through Y2H and LCI assays that OsNINJA3 interacts with various OsJAZ proteins, including OsJAZ6 (Extended Data Fig. 8). OsNINJA1 has been reported to interact with TPR1/3 to inhibit downstream gene expression[45,46]. The formation of complexes with OsJAZ proteins enables OsNINJA3 to inhibit JA-responsive gene expression by recruiting the corepressor TPL/TPR. Moreover, CP enhanced the ability of RBRL to reverse this inhibition by degrading the OsNINJA3 protein (Fig. 5d). The NINJA3 protein level was lower in the *CP*-OE rice plants than in the NPB plants (Fig. 5d).

We also investigated the role of *OsNINJA3* in rice antiviral defence by inoculating *OsNINJA3*-related rice lines with small brown planthopper-carrying viruses. The *ninja3*-mutant lines displayed milder disease symptoms after infection with RSV compared with the *NINJA3*-OE lines and NPB plants (Fig. 5e,f and Supplementary Table 3). Moreover, the levels of viral RNA and CP accumulation were significantly lower in the *ninja3*-mutant lines (Fig. 5g,h). Conversely, overexpression of *OsNINJA3* exacerbated the RSV infection symptoms and disease progression (Fig. 5e,f and Supplementary Table 3). These plants exhibited more severe symptoms and increased viral RNA and CP accumulation (Fig. 5g,h).

Given that OsRBRL interacts with OsNINJA1/2/3, to verify the roles of OsNINJA1 and OsNINJA2 in rice antiviral defence, we also obtained a *ninja1*-mutant (*modd-2*)[46] (Extended Data Fig. 9a), along with the *OsNINJA2*-knockout mutant (Extended Data Fig. 9e) and *OsNINJA2* overexpression (*NINJA2*-OE) lines. In response to natural RSV infection, the disease symptoms of the *ninja1* mutants were similar to those of the wild-type Dongjing (DJ) plants (Extended Data Fig. 9b,c and Supplementary Table 3). Compared with that in DJ plants, CP accumulation in *ninja1* mutants was not significantly different (Extended Data Fig. 9d). Compared with the NPB plants, the *ninja2*-mutant and *NINJA2*-OE rice plants presented similar disease symptoms and CP accumulation (Extended Data Fig. 9f–h and Supplementary Table 3). We also generated *ninja1/2/3* triple mutants in the *ninja3* single-mutant background (Extended Data Fig. 9i). The resistance of the *ninja1/2/3* triple mutants to RSV infection was comparable to that of the *ninja3* single mutant (Extended Data Fig. 9j,k). These data indicated that, in contrast to *OsNINJA3*, *OsNINJA1* and *OsNINJA2* do not have a major role in rice antiviral defence against RSV.

Previous studies have shown that OsAGO18 releases OsAO through competitive binding of miR528 to OsAGO1, thereby increasing ROS levels to defend against viruses. We therefore measured the levels of OsAO protein and ROS in NPB and *rbrl*- and *ninja3*-mutant plants. OsAO levels were reduced in the *rbrl* mutants (Extended Data Fig. 9l) and increased in the *ninja3* mutants (Extended Data Fig. 9m) compared with those

in the NPB plants. Consistently, the ROS levels were lower in the *rbrl* mutants and higher in the *ninja3* mutants (Extended Data Fig. 9n,o).

Overall, the absence or RBRL-mediated degradation of OsNINJA3 relieves its repression of the JA signalling pathway, elevates the expression of *OsAGO18* and, ultimately, strengthens the defence of rice hosts against viral infection.

RBRL mediates broad-spectrum resistance

Recent studies have shown that the activation of JA signalling and the RNAi pathway mediates antiviral defence against different rice viruses[47,48]. We wondered whether the perception of viral effectors by RBRL induces the initiation of the universal antiviral defence of plants. RNA-seq data from a previous study showed that rice dwarf virus (RDV) infection also activates JA biosynthesis and signalling in rice[49] (Extended Data Fig. 10a). RDV is a member of the *Phytoreovirus* genus[50]. We tested whether RBRL could also interact with RDV-encoded proteins through Y2H assays. The RDV coat proteins P2 and P9 interacted with RBRL (Extended Data Fig. 10b). MST assays showed that the K_d between P2 and RBRL is 183.47 nM (Extended Data Fig. 10c). Like RSV CP, P2 and P9 are not substrates of RBRL (Extended Data Fig. 4h,i), indicating that the same mechanism of RBRL-mediated antiviral activity against RDV occurs. We therefore challenged NPB and JA signalling-related rice lines with RDV through natural infection experiments using viruliferous leafhoppers (*Nephotettix cincticeps*), the transmission vector of RDV. We categorized the RDV-induced disease symptoms into four classes based on severity (Extended Data Fig. 10d). Compared with the NPB plants, the *coi1-13*, *jamyb* and *rbrl* rice mutants were more susceptible to infection, whereas the *JAMYB*-OE and *RBRL*-OE rice lines showed increased resistance[17] (Extended Data Fig. 10e–j and Supplementary Table 3). Consistently, the viral RNA and protein levels were increased in the *rbrl* mutants and decreased in the *RBRL*-OE rice plants (Extended Data Figs. 4j and 10k–l). These results underscore the pivotal role of *OsRBRL* in strengthening broad-spectrum rice antiviral defences.

Overall, our study revealed a fundamental mechanism by which rice plants respond to viral infections. This mechanism centres on the perception of viral CP by the RBR-type E3 ligase RBRL, which functions as a sensor for the subsequent antiviral defence in the host. After RSV infection, CP is perceived by OsRBRL to facilitate the degradation of OsNINJA3, a negative regulator of the JA signalling pathway, and this degradation process is orchestrated by the ubiquitination activity of OsRBRL. The degradation of OsNINJA3 activates the JA signalling pathway, leading to increased JA biosynthesis and upregulation of *OsAGO18* expression. These events occur independently of COI1-mediated JA signalling responses. With the accumulation of JA, COI1-mediated JA signalling establishes a positive-feedback loop, amplifying the expression of *OsAGO18* to a sufficiently high level. This increased expression of *OsAGO18* enhances the host antiviral defence by alleviating the repression of AGO1-mediated antiviral RNAi and promoting the upregulation of ROS levels by AO, as previously reported[17–19] (Extended Data Fig. 10m). Thus, our study provides deeper insights into the intricacies of the molecular processes that underlie how plants perceive viral infections and initiate antiviral immune defence against viral infections and therefore establishes a foundation for further exploration in this field.

Discussion

In addition to viral assembly, CP also acts as an effector to induce plant immunity[17–19]. CP-mediated antiviral defence has been studied for half a century, but the underlying mechanisms, especially the initiation process, remain largely unclear. As most plant viruses are naturally transmitted by insect vectors, viruses are usually directly injected inside host cells when viruliferous insects feed on host. How plant hosts perceive viral infections is an intriguing question, and observing and testing viruses in plant systems are challenging. However, the vast majority of studies on plant antiviral defence mechanisms have used artificial infection methods, such as mechanical inoculation with in vitro viral RNA transcripts or virions or infiltration of agrobacteria containing engineered viral DNA. These methods often yield markedly greater inoculum levels compared with those that occur under natural infection, and the potential influence of these methods on the plant immune response remains an unanswered question. Here we used natural viral insect vectors to initiate infection, which best reflects the infection process under field conditions regarding the behaviour of viruses and the host response. This approach is important not only for the dissection of virus–host interactions but also for further design of disease-resistance breeding programs.

JA is a key immune hormone that enhances the resistance of plants to diverse threats, from microbial pathogens to various herbivores[51,52]. The core pathways governing the biosynthesis and signalling of JA in plants have been extensively studied in recent decades[52,53]. Moreover, the importance of post-translational modifications in the fine-tuning of JA responses across diverse spatiotemporal scales has just been revealed[54–57]. Here we identified a derepression mechanism for JA-mediated antiviral signalling through the OsRBRL-mediated ubiquitination and degradation of OsNINJA3. OsNINJA1 and OsNINJA2 display almost no effects on antiviral defence, although they also interact with OsRBRL, which indicates that there is little redundancy among these OsNINJA proteins during rice antiviral defence. These functional differences among NINJA adaptors could be the result of evolutionary divergence.

Results from HHARI and TRIAD proteins, orthologues of OsRBRL, indicate that binding by their interactors could release their autoinhibition by opening the mask of the Ariadne domain on the active site[39,43]. RSV CP–RBRL interaction promotes RBRL self-ubiquitination and RBRL-mediated ubiquitination of NINJA3 in bacterial systems. Thus, CP appears to release the autoinhibition of OsRBRL, possibly through interaction, thereby exposing the active site. Notably, we found that CP-mediated degradation and activation of RBRL varies with context, similar to Keep on Going, a previously reported E3 ubiquitin ligase[58]. When co-expressing RBRL and CP in tobacco leaves, CP primarily promotes the degradation of RBRL. Meanwhile, in RSV-infected rice or when co-expressing RBRL with CP and OsNINJA3 in tobacco leaves, CP facilitates the degradation of NINJA3 by RBRL.

Overall, our findings reveal a fundamental mechanism by which plant hosts perceive viral infection and initiate subsequent antiviral defence responses through the RBR-type E3 ligase and will facilitate diverse research in the broader field of plant immunity.

Online content

Any methods, additional references, Nature Portfolio reporting summaries, source data, extended data, supplementary information, acknowledgements, peer review information; details of author contributions and competing interests; and statements of data and code availability are available at https://doi.org/10.1038/s41586-025-08706-8.

1. Gong, Q. et al. Molecular basis of methyl-salicylate-mediated plant airborne defence. *Nature* **622**, 139–148 (2023).
2. Xia, J. et al. Whitefly hijacks a plant detoxification gene that neutralizes plant toxins. *Cell* **184**, 1693–1705 (2021).
3. Baulcombe, D. RNA silencing in plants. *Nature* **431**, 356–363 (2004).
4. Guo, Z., Li, Y. & Ding, S.-W. Small RNA-based antimicrobial immunity. *Nat. Rev. Immunol.* **19**, 31–44 (2019).
5. Yang, Z. & Li, Y. Dissection of RNAi-based antiviral immunity in plants. *Curr. Opin. Virol.* **32**, 88–99 (2018).
6. Jones, J. D. G. & Dangl, J. L. The plant immune system. *Nature* **444**, 323–329 (2006).
7. Zhou, W. et al. A jasmonate signaling network activates root stem cells and promotes regeneration. *Cell* **177**, 942–956 (2019).
8. Castillo-González, C. et al. Geminivirus-encoded TrAP suppressor inhibits the histone methyltransferase SUVH4/KYP to counter host defense. *eLife* **4**, e06671 (2015).
9. Muthayya, S., Sugimoto, J. D., Montgomery, S. & Maberly, G. F. An overview of global rice production, supply, trade, and consumption. *Ann. N. Y. Acad. Sci.* **1324**, 7–14 (2014).

10. Wang, Q. et al. STV11 encodes a sulphotransferase and confers durable resistance to rice stripe virus. *Nat. Commun.* **5**, 4768 (2014).
11. Wu, J. et al. Current rice production is highly vulnerable to insect-borne viral diseases. *Natl Sci. Rev.* **9**, nwac131 (2022).
12. Ye, J., Zhang, L., Zhang, X., Wu, X. & Fang, R. Plant defense networks against insect-borne pathogens. *Trends Plant Sci.* **26**, 272–287 (2021).
13. Du, P. et al. Viral infection induces expression of novel phased microRNAs from conserved cellular microRNA precursors. *PLoS Pathog.* **7**, e1002176 (2011).
14. Wang, Y. et al. A calmodulin-binding transcription factor links calcium signaling to antiviral RNAi defense in plants. *Cell Host Microbe* **29**, 1393–1406 (2021).
15. Zhou, J.-M. & Zhang, Y. Plant immunity: danger perception and signaling. *Cell* **181**, 978–989 (2020).
16. Kourelis, J., Marchal, C., Posbeyikian, A., Harant, A. & Kamoun, S. NLR immune receptor-nanobody fusions confer plant disease resistance. *Science* **379**, 934–939 (2023).
17. Yang, Z. et al. Jasmonate signaling enhances RNA silencing and antiviral defense in rice. *Cell Host Microbe* **28**, 89–103 (2020).
18. Wu, J. et al. Viral-inducible argonaute 18 confers broad-spectrum virus resistance in rice by sequestering a host microRNA. *eLife* **4**, e05733 (2015).
19. Wu, J. et al. ROS accumulation and antiviral defence control by microRNA528 in rice. *Nat. Plants* **3**, 16203 (2017).
20. Zhu, H. et al. *Arabidopsis* argonaute 10 specifically sequesters miR166/165 to regulate shoot apical meristem development. *Cell* **145**, 242–256 (2011).
21. Zhai, Q., Yan, C., Li, L., Xie, D. & Li, C. in *Hormone Metabolism and Signaling in Plants* (eds Li, J. et al.) 243–272 (Academic, 2017).
22. Wu, D. et al. Viral effector protein manipulates host hormone signaling to attract insect vectors. *Cell Res.* **27**, 402–415 (2017).
23. Chini, A. et al. The JAZ family of repressors is the missing link in jasmonate signalling. *Nature* **448**, 666–671 (2007).
24. Pauwels, L. et al. NINJA connects the co-repressor TOPLESS to jasmonate signalling. *Nature* **464**, 788–791 (2010).
25. Sheard, L. B. et al. Jasmonate perception by inositol-phosphate-potentiated COI1–JAZ co-receptor. *Nature* **468**, 400–405 (2010).
26. Thines, B. et al. JAZ repressor proteins are targets of the SCF^{COI1} complex during jasmonate signalling. *Nature* **448**, 661–665 (2007).
27. Du, M. et al. MYC2 orchestrates a hierarchical transcriptional cascade that regulates jasmonate-mediated plant immunity in tomato. *Plant Cell* **29**, 1883–1906 (2017).
28. Yan, C. et al. Injury activates Ca^{2+}/calmodulin-dependent phosphorylation of JAV1–JAZ8–WRKY51 complex for jasmonate biosynthesis. *Mol. Cell* **70**, 136–149 (2018).
29. Bittner, A. et al. Organelles and phytohormones: a network of interactions in plant stress responses. *J. Exp. Bot.* **73**, 7165–7181 (2022).
30. Zhai, Q., Deng, L. & Li, C. Mediator subunit MED25: at the nexus of jasmonate signaling. *Curr. Opin. Plant Biol.* **57**, 78–86 (2020).
31. Vierstra, R. D. The ubiquitin–26S proteasome system at the nexus of plant biology. *Nat. Rev. Mol. Cell Biol.* **10**, 385–397 (2009).
32. Jiang, X. & Chen, Z. J. The role of ubiquitylation in immune defence and pathogen evasion. *Nat. Rev. Immunol.* **12**, 35–48 (2012).
33. Buetow, L. & Huang, D. T. Structural insights into the catalysis and regulation of E3 ubiquitin ligases. *Nat. Rev. Mol. Cell Biol.* **17**, 626–642 (2016).
34. Li, H. et al. Rift Valley fever virus coordinates the assembly of a programmable E3 ligase to promote viral replication. *Cell* **187**, 6896–6913 (2024).
35. Pertel, T. et al. TRIM5 is an innate immune sensor for the retrovirus capsid lattice. *Nature* **472**, 361–365 (2011).
36. Liu, L. et al. OsRFPH2-10, a RING-H2 finger E3 ubiquitin ligase, is involved in rice antiviral defense in the early stages of rice dwarf virus infection. *Mol. Plant* **7**, 1057–1060 (2014).
37. Duda, D. M. et al. Structure of HHARI, a RING-IBR-RING ubiquitin ligase: autoinhibition of an Ariadne-family E3 and insights into ligation mechanism. *Structure* **21**, 1030–1041 (2013).
38. Wenzel, D. M., Lissounov, A., Brzovic, P. S. & Klevit, R. E. UBCH7 reactivity profile reveals parkin and HHARI to be RING/HECT hybrids. *Nature* **474**, 105–108 (2011).
39. Spratt, D. E., Walden, H. & Shaw, G. S. RBR E3 ubiquitin ligases: new structures, new insights, new questions. *Biochem. J* **458**, 421–437 (2014).
40. Eisenhaber, B., Chumak, N., Eisenhaber, F. & Hauser, M.-T. The ring between ring fingers (RBR) protein family. *Genome Biol.* **8**, 209 (2007).
41. Zhou, B. & Zeng, L. Conventional and unconventional ubiquitination in plant immunity. *Mol. Plant Pathol.* **18**, 1313–1330 (2017).
42. Han, Y. et al. Reconstitution of the plant ubiquitination cascade in bacteria using a synthetic biology approach. *Plant J.* **91**, 766–776 (2017).
43. Scott, D. C. et al. Two distinct types of E3 ligases work in unison to regulate substrate ubiquitylation. *Cell* **166**, 1198–1214 (2016).
44. Hong, S. A.-O. et al. Heterologous microProtein expression identifies LITTLE NINJA, a dominant regulator of jasmonic acid signaling. *Proc. Natl Acad. Sci. USA* **117**, 26197–26205 (2020).
45. Kashihara, K. et al. Overexpression of *Os*NINJA1 negatively affects a part of *Os*MYC2-mediated abiotic and biotic responses in rice. *J. Plant Physiol.* **232**, 180–187 (2019).
46. Tang, N. et al. MODD mediates deactivation and degradation of *Os*bZIP46 to negatively regulate ABA signaling and drought resistance in rice. *Plant Cell* **28**, 2161–2177 (2016).
47. Zhang, C. et al. Suppression of jasmonic acid-mediated defense by viral-inducible microRNA319 facilitates virus infection in rice. *Mol. Plant* **9**, 1302–1314 (2016).
48. Tan, X. et al. NF-YA transcription factors suppress jasmonic acid-mediated antiviral defense and facilitate viral infection in rice. *PLoS Pathog.* **18**, e1010548 (2022).
49. Zhao, S. et al. A viral protein promotes host SAMS1 activity and ethylene production for the benefit of virus infection. *eLife* **6**, 27529 (2017).
50. Qin, Q. et al. Auxin response factors (ARFs) differentially regulate rice antiviral immune response against rice dwarf virus. *PLoS Pathog.* **16**, e1009118 (2020).
51. Yang, Z. et al. Crop antiviral defense: past and future perspective. *Sci. China Life Sci.* **67**, 2617–2634 (2024).
52. Howe, G. A., Major, I. T. & Koo, A. J. Modularity in jasmonate signaling for multistress resilience. *Annu. Rev. Plant Biol.* **69**, 387–415 (2018).
53. Wasternack, C. & Hause, B. Jasmonates: biosynthesis, perception, signal transduction and action in plant stress response, growth and development. An update to the 2007 review in *Annals of Botany*. *Ann. Bot.* **111**, 1021–1058 (2013).
54. An, C. et al. Regulation of jasmonate signaling by reversible acetylation of TOPLESS in *Arabidopsis*. *Mol. Plant* **15**, 1329–1346 (2022).
55. Chico, J. M. et al. $CUL3^{BPM}$ E3 ubiquitin ligases regulate MYC2, MYC3, and MYC4 stability and JA responses. *Proc. Natl Acad. Sci. USA* **117**, 6205–6215 (2020).
56. Srivastava, A. K. et al. SUMO suppresses the activity of the jasmonic acid receptor CORONATINE INSENSITIVE1. *Plant Cell* **30**, 2099–2115 (2018).
57. Zhu, T. et al. Warm temperature triggers JOX and ST2A-mediated jasmonate catabolism to promote plant growth. *Nat. Commun.* **12**, 4804 (2021).
58. Liu, H. & Stone, S. Abscisic acid increases *Arabidopsis* ABI5 transcription factor levels by promoting KEG E3 ligase self-ubiquitination and proteasomal degradation. *Plant Cell* **22**, 2630–2641 (2010).

Methods

Rice plants and growth conditions

We used the rice ecotype NPB or DJ as the wild-type control. The *coi1-13* mutant was identified by quantitative PCR with reverse transcription (RT–qPCR) and phenotypic observation, consistent with previous reports[59]. The *jamyb* mutant was identified by sequencing, as previously described[17]. The *ninja1* (*modd-2*) mutant was identified by genotyping using gene-specific and T-DNA-specific primers as described previously[46]. All of the rice plants were cultivated in a greenhouse at 28–32 °C and at a relative humidity of 60 ± 5%.

N. benthamiana growth conditions

N. benthamiana plants were cultivated in soil within a greenhouse under a 16 h–8 h light–dark photoperiod at a constant temperature of 24 °C. For transient expression assays, the upper three leaves of 1-month-old plants were used.

Vector construction and rice transformation

The coding sequences of *OsRBRL*, RSV *CP*, *OsNINJA2* and *OsNINJA3* were initially amplified by RT–PCR. Subsequently, the genes were individually cloned and inserted into the pCambia2300-Actin1-OCS and pCambia2300-Actin1-3×MYC vectors, resulting in the generation of the *Actin1::HA-OsRBRL*, *Actin1::HA-CP*, *Actin1::3×MYC-OsNINJA2* and *Actin1::3×MYC-OsNINJA3* constructs. The *rbrl*-, *ninja2*-, *ninja3*- and *ninja1/2/3*-knockout lines were generated using CRISPR–Cas9 according to established protocols[60]. These constructs were subsequently introduced into wild-type NPB plants or *rbrl* 2 mutant plants through *Agrobacterium tumefaciens*-mediated transformation using a process facilitated by BioRun and BIOGLE GeneTech. The rice lines overexpressing *OsRBRL*, RSV *CP* and *OsNINJA3* were verified by immunoblotting. The genome-edited mutants were confirmed by sequencing and analysed using SnapGene (https://www.snapgene.com). For transient expression assays, genes in recombinant binary vectors were initially amplified by RT–PCR and subsequently cloned and inserted into the corresponding entry vectors pEASY-Blunt-Simple and pENTR/D-TOPO. These inserts were subsequently cut and either ligated or recombined into destination vectors. Detailed primer information is provided in Supplementary Table 5.

Immunoblotting and quantification analysis

Plant samples were homogenized in liquid nitrogen, and total proteins were extracted from equal weights of ground powder using the same volume of 2× Laemmli buffer (4% (w/v) SDS, 20% (v/v) glycerol, 10% (v/v) 2-mercaptoethanol, 0.004% (w/v) bromophenol blue and 0.125 M Tris-HCl, pH 6.8) and subsequently boiled at 95 °C for 10 min. The supernatants were collected by centrifugation at 12,000 rpm for 5 min and separated by SDS–PAGE. The PageRuler Prestained Protein Ladder (Thermo Fisher Scientific) and Prestained Protein Ladder (Meilun Biotech) were used as molecular mass standards. The proteins were subsequently transferred to nitrocellulose membranes and detected with antibodies against CM-LOX2 (1:2,000)[17], AOS2 (1:2,000)[17], RSV CP (1:5,000)[61], RDV P2 (1:5,000)[62], AGO18 (1:500)[18], AO (1:500)[19], RBRL (1:500), NINJA3 (1:500), MYC (ABclonal, 1:2,000), HA (ABclonal, 1:2,000), GFP/YFP (ABclonal, 1:2,000), GST (ABclonal, 1:2,000), MBP (ABclonal, 1:2,000), Flag (TransGen Biotech, 1:2,000), S (EarthOx, 1:2,000), FBPA (Beijing Protein Innovation, 1:2,000), histone H3 (Abcam, 1:2,000), cLUC (Sigma-Aldrich, 1:1,000) and actin (CWBIO, 1:10,000). Actin was used as the loading control or sample processing control. Images from immunoblotting were collected using the Molecular Imager ChemiDoc XRS+ (Bio-Rad) system. The corresponding band intensities were quantified using ImageJ (https://imagej.net/ij/). The band intensities for a particular protein were normalized to those for actin or Rubisco. Relative values were calculated by comparison with the first band on the left in each figure. Uncropped immunoblotting images are provided in Supplementary Fig. 1.

Nuclear–cytoplasmic fractionation followed by an immunoprecipitation assay

To precisely screen for rice proteins that interact with RSV CP in the nucleus, we performed nuclear–cytoplasmic fractionation followed by IP–MS on RSV-infected NPB and *CP*-OE rice, with mock NPB rice used as a control. First, we conducted subcellular fractionation on the rice materials with minor modifications as described previously[63]. The rice materials were harvested and ground into powder in liquid nitrogen at 4 weeks after RSV infection. The powder (approximately 1 g) was resuspended in Honda buffer (0.4 M sucrose, 2.5% Ficoll, 5% dextran T40, 25 mM Tris-HCl (pH 7.4), 10 mM $MgCl_2$, 0.5% Triton X-100, 0.5 mM PMSF, 10 mM β-mercaptoethanol, RNase inhibitor and Roche protease inhibitor cocktail) at a ratio of 2 ml g^{-1}. The homogenate was filtered twice through a double-layered Miracloth, and the supernatant was subsequently centrifuged at 1,500*g* for 5 min at 4 °C. The supernatant was further centrifuged at 10,000*g* for 10 min at 4 °C to obtain the cytoplasmic fraction. The pellet containing the nuclear proteins was resuspended in three volumes of nuclear extraction buffer (500 mM KCl, 20 mM Tris-HCl (pH 8.0), 0.5% Triton X-100, 25% glycerol, 1.5 mM $MgCl_2$, 0.5 mM EDTA, 1 mM dithiothreitol (DTT), cocktail and 1 mM PMSF) and incubated for 30 min at 4 °C. Insoluble nuclear residues were then sedimented at 10,000*g* at 4 °C for 10 min, and the supernatant was collected for the IP assay. The nuclear extract was diluted with four volumes of dilution buffer (20 mM Tris-HCl (pH 8.0), 500 mM KCl, 0.5% Triton X-100, 1 mM $MgCl_2$, 0.5 mM EDTA, 1 mM DTT, cocktail and 1 mM PMSF). The mixture was precleared with protein G for 30 min, and 1:100 anti-CP antibody was then added and incubated for 2 h, followed by the addition of 1:200 protein G and further incubation for 2 h. The samples were washed three times with washing buffer (20 mM Tris-HCl (pH 8.0), 500 mM KCl, 0.5% Triton X-100, 5% glycerol, 1 mM $MgCl_2$, 0.5 mM EDTA, 1 mM DTT, cocktail and 1 mM PMSF). Finally, the bead-bound proteins were eluted in 2× Laemmli buffer and subjected to SDS–PAGE. For LC–MS/MS analysis, the gel was subjected to silver staining to identify the candidate CP-interacting proteins.

IP for LC–MS/MS assay

IP–LC–MS/MS assays were performed as previously described with some modifications[64,65]. To detect proteins that interact with RBRL, we performed IP-LC–MS/MS assays with transgenic plants that overexpressed HA-tagged versions of RBRL. In brief, rice samples were homogenized in liquid nitrogen. Total proteins were extracted from 200 mg of ground powder using IP buffer (50 mM Tris-HCl (pH 7.4), 150 mM NaCl, 4 mM $MgCl_2$, 0.5% (v/v) NP-40, 5 mM DTT, 1 mM phenylmethylsulfonyl fluoride, 50 μM MG132 and 1× protease inhibitor cocktail) and then incubated for 30 min at 4 °C with gentle rotation. Next, the samples were centrifuged at 12,000 rpm and 4 °C three times for 5 min each; the supernatants were collected after each centrifugation step. The resulting supernatant was transferred to a new tube containing 7.5 μl of HA-magnetic agarose (MBL) and incubated at 4 °C for 2.5 h with gentle rotation. The samples were then washed three times with wash buffer A (50 mM Tris-HCl (pH 7.4), 150 mM NaCl and 4 mM $MgCl_2$). Finally, the bead-bound proteins were eluted in 2× Laemmli buffer and subjected to SDS–PAGE. For LC–MS/MS analysis, the gel was subjected to silver staining to identify the candidate RBRL-interacting proteins.

LC–MS/MS assay

First, the gel was cut into small pieces and placed into tubes for digestion. A total of 400 μl of decolourization solution was added to each tube and shaken until completely decolorized, after which the liquid was discarded. Next, 400 μl of acetonitrile was added, and the mixture was shaken until the gel pieces turned white; the liquid was then discarded. Next, 200 μl of 10 mM DTT and 25 mM NH_4HCO_3 were added,

and the mixture was incubated at 56 °C for 1 h. The mixture was cooled to room temperature, the liquid was discarded, 200 µl of 55 mM IAM and 25 mM NH_4HCO_3 were added, and the mixture was incubated in the dark for 45 min. After the liquid in the tubes was discarded, the gels were washed twice with 25 mM NH_4HCO_3. Next, 400 µl of acetonitrile was added, and the mixture was shaken until the gel pieces turned white. The liquid was discarded, and the gel pieces were crushed with a pipette tip. For each tube, trypsin was added to 25 mM NH_4HCO_3 buffer at a trypsin ratio of 1:50 (w/w), and the mixture was subsequently incubated at 37 °C overnight. Then, 200 µl of acetonitrile containing 0.1% formic acid was added to each tube, the tubes were shaken for 10 min and the supernatant was then transferred to a clean tube. Next, 30 µl of 0.1% formic acid was added to the gel, which was shaken for 10 min, then 200 µl of acetonitrile containing 0.1% formic acid was added and the mixture was shaken for another 10 min. The supernatant was collected and dried using a vacuum centrifuge. Peptide samples were dissolved in 0.1% formic acid solution to a concentration of approximately 0.1 µg µl^{-1}. The mixture was centrifuged at 16,700*g* for 12 min, and the supernatant was transferred to a MS injection vial to conduct the LC–MS/MS assay. LC–MS/MS analysis was performed using the EASY-nLC 1200 liquid chromatography system and a C18 column coupled with a Thermo Fusion Lumos mass spectrometer. The mobile phase for liquid chromatography consisted of 0.1% formic acid (phase A) and 80% acetonitrile/0.1% formic acid (phase B). The flow rate was set at 280 nl min^{-1}. The LC–MS/MS results were processed using Proteome Discoverer 2.2 software and the rice database to acquire the CP- and RBRL-interacting proteins.

Transient expression in *N. benthamiana* leaves

Agrobacterium-mediated transient expression assays were performed as previously described[17] with minor modifications. The recombinant binary vectors were subsequently transformed into *A. tumefaciens* strain GV3101 using the freeze–thaw method. Suspensions of *Agrobacterium* cultures were adjusted to an optical density at 600 nm (OD_{600}) of 1.0 and used to infiltrate leaves of *N. benthamiana* plants at the four- to five-leaf stage through a 1-ml syringe without a needle. Leaf tissues were harvested at 2 days after agroinfiltration.

LCI assay

LCI assays were also conducted as previously described[17]. The coding sequences of *OsRBRL*, RSV *CP*, four *OsNINJA* genes and *OsRBRL-like*, and the RBR NTD domain, RBR RBR domain, RBR Ari domain, NINJA3 EAR domain, NINJA3 NINJA-B domain, NINJA3 ZBD NTE domain and NINJA3 ZBD core domain and all OsJAZ genes were separately inserted into the pCambia1300-nLUC or pCambia1300-cLUC vectors. A list of the primers used is provided in Supplementary Table 5. All of the constructs were subsequently transformed into *A. tumefaciens* strain GV3101 using the freeze–thaw method. Four combinations of *A. tumefaciens* suspensions were mixed, adjusted to a final concentration with an OD_{600} of 1.0 and coinfiltrated into four different regions on the same *N. benthamiana* leaf. At 2 days after agroinfiltration, cells were infiltrated with 200 µM luciferin (Promega), and luciferase activity was detected using a low-light cooled charge-coupled device imaging apparatus (NightOWL II LB983 with IndiGO software v.2.0.4.0). At least three biological replicates were performed.

Co-IP assay

35S::YFP-CP was constructed by inserting the coding sequence of RSV *CP* into the pEarleyGate104 vector and was subsequently used to express YFP–CP. *35S::HA-RBRL* was constructed by fusing the coding sequence of *OsRBRL* into the pCambia2300 vector and was subsequently used to express HA–RBRL. pCambia1301-35S-GFP was used to express GFP. All of the constructs were subsequently transformed into *A. tumefaciens* strain GV3101 using the freeze–thaw method. The indicated combinations of *A. tumefaciens* suspensions were mixed to a final concentration with an OD_{600} of 1.0. The infiltration procedures were performed as described above (see the 'Transient expression in *N. benthamiana* leaves' section). Leaves were harvested at 2 days after agroinfiltration, and total proteins were extracted with native extraction buffer (50 mM Tris-MES (pH 8.0), 500 mM sucrose, 1 mM $MgCl_2$, 10 mM EDTA, freshly added 5 mM DTT and 1× protease inhibitor cocktail)[66]. The mixture was incubated at 4 °C for 30 min with gentle rotation and then centrifuged at 12,000 rpm and 4 °C three times for 10 min each; the supernatants were collected after each centrifugation step. Cleared extracts were immunoprecipitated using GFP-tagged or HA-tagged Nanoselector Agarose (HUABIO) and incubated for 1 h at 4 °C with gentle rotation. The samples were then washed three times with washing buffer B (10 mM Tris-HCl (pH 7.5), 150 mM NaCl and 0.5 mM EDTA). Finally, the bead-bound proteins were eluted in 2× Laemmli buffer. The eluted proteins were boiled for 10 min, centrifuged, separated by SDS–PAGE and detected with antibodies against HA (ABclonal) and GFP (ABclonal).

Protein expression and purification

The coding sequences of RSV *CP*, RDV *P2*, RDV *P2*$^{1–786}$, RDV *P9*, *OsRBRL* and four *OsNINJA* genes were inserted into the pHM4 (MBP tag, modified from pMAL-c2X Vector, New England Biolabs), pGEX4T1 (GST tag, GE Healthcare), pACYCDuet[42] or pCDFDuet[42] vector and expressed as tag fusion proteins (MBP–RBRL, GST–CP, GST–NINJA1, GST–NINJA2, GST–NINJA3, GST–NINJA4, RBRL–MYC, MBP–P2–HA, MBP–P9–HA, MBP–P2$^{1–786}$ and MBP–NINJA3–HA) in *E. coli* strain Transetta or BL21 (DE3; TransGen Biotech). The fusion proteins were purified using glutathione Sepharose 4B beads (GE Healthcare) or amylose resin (New England Biolabs) or detected by immunoblotting as previously described[42].

Pull-down assay

Equimolar amounts of MBP–RBRL on MBP tag Nanoselector Agarose (HUABIO) were separately incubated with equal amounts of GST, GST–CP, GST–NINJA1, GST–NINJA2, GST–NINJA3 or GST–NINJA4 in pull-down buffer (20 mM Tris-HCl (pH 7.5), 200 mM NaCl) at 4 °C for 1 h with gentle rotation. The beads were then washed (five times for 5 min each) with pull-down buffer (containing 2% (v/v) Triton X-100). The bound proteins were boiled in 2× Laemmli buffer, separated by SDS–PAGE, and detected with antibodies against MBP (ABclonal) and GST (ABclonal).

Virus inoculation

The virus inoculation procedures were performed as previously described[17,67]. In brief, 2-week-old rice plants were inoculated with two viruliferous (containing RSV or RDV) or virus-free (mock) insects. Then, 2 days after inoculation, the insects were removed, and the rice plants were returned to the greenhouse as described above (see the 'Rice plants and growth conditions' section). The inoculated plants were monitored weekly for the appearance of viral symptoms. The numbers of rice plants of each line with various disease symptom grades were recorded at 4 w.p.i. (Supplementary Table 3). Photographs of plants with representative symptoms were acquired at 2 or 4 w.p.i.; whole shoots were harvested for RT–qPCR and immunoblotting assays at 4 w.p.i.

RNA extraction and RT–qPCR analysis

Rice samples were homogenized in liquid nitrogen, and total RNA was extracted from 100 mg of ground powder using TRIzol Reagent (Thermo Fisher Scientific) in accordance with the manufacturer's instructions. Total RNA was treated with RQ1 RNase-free DNase (Promega) to remove traces of contaminating genomic DNA. The RNA was subsequently reverse-transcribed using M-MLV reverse transcriptase (Promega), oligo$(dT)_{18}$ primer and recombinant RNasin ribonuclease inhibitor (Promega) according to the manufacturer's instructions. The resulting cDNA was used as the template for RT–PCR and RT–qPCR. RT–qPCR was performed using the SYBR Green Real-Time PCR Master Mix (Mei5 Biotech) according to the manufacturer's instructions using

the Bio-Rad CFX96 system with CFX Maestro 1.1 software. The level of *OsEF-1a* expression was detected in parallel and used as the internal control. A list of the primers used is provided in Supplementary Table 5.

Phylogenetic analysis

The amino acid sequences of RBRL, other RBR family proteins, and NINJA family proteins were obtained from UniProt (https://www.uniprot.org/). An unrooted, neighbour-joining tree was constructed using Molecular Evolutionary Genetic Analysis 11 (MEGA11).

Generation of rice RBRL and NINJA3 antibodies

Rabbit polyclonal antibodies were generated by HUABIO or ABclonal. The synthetic peptides RBRL (DLHLRLPDDRPADC) and NINJA3 (STGKPLNGTVTQQS) were used to obtain rabbit polyclonal antibodies to RBRL and NINJA3, respectively. The antisera were affinity-purified and used for immunoblotting.

Sample preparation and JA quantitative assay

Hormone extractions and measurements of the JA concentration were performed as previously described[68]. In brief, rice shoots from 2-week-old NPB, *rbrl* and *RBRL*-OE plants were separately collected and ground into fine powder. JA was extracted from 110 mg of ground powder using 400 µl of 10% methanol containing 1% acetic acid and then purified with a 0.22-µm nylon filter. The eluate was analysed by ultra-high-performance liquid chromatography–triple quadrupole MS (UPLC–MS/MS) on a mass spectrometer (UPLC 1290-MS/MS 6495).

In vivo and semi-in vivo protein degradation

In vivo and semi-in vivo protein degradation experiments were conducted as previously described[66]. For in vivo protein degradation experiments, agrobacterial strains containing *35S::HA-RBRL*, *35S::HA-RBRL-like*, *35S::YFP-NINJA3*, *35S::YFP-NINJA4*, *35S::FLAG-GUSA* (internal control) or *35S::MYC-CP* were coinfiltrated at the indicated ratios. The infiltration procedures were performed as described above (see the 'Transient expression in *N. benthamiana* leaves' section). Then, 2 days after infiltration, the samples were collected for analysis. For semi-in vivo protein degradation experiments, agrobacterial strains containing *35S::HA-RBRL*, *35S::YFP-NINJA3*, *35S::YFP-NINJA4*, *35S::GFP*, *35S::YFP-CP* or pCambia2300 (empty vector) were infiltrated separately. The infiltration procedures were performed as described above (see the 'Transient expression in *N. benthamiana* leaves' section). Then, 2 days after infiltration, the samples were collected separately and extracted using native extraction buffer (containing 10 µM ATP). An equal volume of the corresponding extracts was mixed together. A final concentration of 50 µM MG132 was added to the corresponding mixture. The mixtures were incubated at 4 °C with gentle rotation. The samples were removed at various timepoints, and the reaction was terminated by the addition of 2× Laemmli buffer and boiling for 5 min; finally, the samples were subjected to immunoblotting analysis.

Y2H assay

The coding sequences of 14 *OsJAZ* genes, 4 *OsNINJA* genes, 12 RDV proteins and *OsRBRL* were separately cloned and inserted into the pDEST-GBKT7 or pDEST-GADT7 vector. A list of the primers used is provided in Supplementary Table 5. Yeast transformation was performed as described by the vector manufacturer (Clontech, Mountain View). Different combinations of constructs were cotransformed into yeast AH109 cells. All yeast transformants were subsequently grown on SD/−Leu/−Trp and subsequently transferred to SD/−Leu/−Trp/−His/−Ade medium for interaction tests.

Transient expression in rice protoplasts

Transient expression in rice protoplasts was conducted as previously described, with some modifications[17,65,69,70]. In brief, the corresponding plasmids were cotransformed into protoplasts using polyethylene glycol (PEG). Rice protoplasts were isolated from the leaf sheaths of 10–14-day-old wild-type (NPB) or *rbrl* 2 plants. The leaf sheaths were initially cut into 0.5-mm pieces with sharp razor blades and then submerged in enzyme solution (0.4 M D-mannitol, 20 mM MES-KOH (pH 5.7), 20 mM KCl, 1.5% cellulase R10 (w/v), 0.7% macerozyme R10 (w/v), 0.1% bovine serum albumin and 10 mM $CaCl_2$) for 7 h with shaking (40 rpm) at 28 °C in the dark. Each sample was filtered through a 40-µm nylon mesh filter. After removal of the enzyme solution, the tissues were suspended in W5 solution (154 mM NaCl, 125 mM $CaCl_2$, 5 mM KCl and 2 mM MES (pH 5.7)) and subsequently filtered through another 40-µm nylon mesh filter. The flow-through samples from the above-mentioned filtrations were mixed and then centrifuged for 3 min at 900 rpm to pellet the protoplasts. The protoplasts were resuspended in W5 solution and incubated on ice for 30 min. The protoplasts were then centrifuged at 900 rpm for 3 min and resuspended at 3×10^5 cells per ml in MMG solution (0.4 M D-mannitol, 15 mM $MgCl_2$ and 4 mM MES-KOH (pH 5.7)) for PEG-mediated transformation. In the transformation, 110 µl of freshly prepared PEG-$CaCl_2$ solution (0.2 M D-mannitol, 100 mM $CaCl_2$ and 40% (v/v) PEG 4000) and 10 µg (10 µl) of plasmid were gently mixed with 100 µl of protoplasts and then incubated for 15 min at room temperature in the dark. After transformation, the cells were washed with 10 volumes of W5 and then resuspended in W1 solution (0.5 M D-mannitol, 4 mM MES-KOH (pH 5.7) and 20 mM KCl) overnight at 28 °C in the dark. The GFP signal was quantified and normalized to the chlorophyll fluorescence, as previously reported[71]. The observation and quantification of each cell were performed under the same set of confocal parameters and at the same scale using LSM710 (Zeiss).

Dual-luciferase reporter system

The dual-luciferase reporter system was established as previously described[17]. In brief, the coding sequences of *OsRBRL* and *OsRBRL-like* were cloned and inserted into the pCambia2300-35S vector. A list of the primers used is provided in Supplementary Table 5. When conducting the assay in tobacco leaves, these two constructs were separately transformed into *A. tumefaciens* strain GV3101 using the freeze–thaw method. The indicated combinations of *A. tumefaciens* suspensions were mixed and adjusted to a final concentration with an OD_{600} of 1.0. The infiltration procedures were performed as described above (see the 'Transient expression in *N. benthamiana* leaves' section). The expression levels of firefly and *Renilla* luciferases in *N. benthamiana* leaves were measured using the GLO-MAX 20/20 luminometer (Promega) at 2 days after agroinfiltration. When conducting the assay in rice protoplasts, these two constructs were co-transformed into rice protoplasts along with *35S::myc-JAZ6*, *35S::GFP*, *35S::YFP-JAMYB*, pCambia2300 (empty vector) and *35S::AGO18pro:LUC* at a fixed ratio. The expression levels of firefly and *Renilla* luciferases in rice protoplasts were measured using the GLO-MAX 20/20 luminometer (Promega) at 12 h after transformation. The ratio of firefly luciferase to *Renilla* luciferase (LUC/REN) was calculated to determine the final transcriptional activity.

Virus isolation and rice protoplast infection

RSV was isolated and purified from rice plants infected with RSV, with some modifications compared to previous studies[10]. Approximately 10 g of leaves that had been stored at −80 °C were blended in 40 ml of phosphate buffer (0.1 M, pH 7.5) containing 0.1% 2-mercaptoethanol, 1% Triton X-100 and 0.01 M EDTA. The homogenate was then filtered through two layers of Miracloth (Millipore), mixed with 20% (v/v) chloroform and stirred for 15 min at room temperature. After centrifugation at 4 °C, 5,000*g* for 20 min for clarification, the supernatant was adjusted to 6% PEG 6,000 and 0.1 M NaCl in an ice bath for 4 h, and then rotated at 4 °C overnight. The resulting precipitate was collected by centrifugation at 4 °C, 5,000*g* for 20 min and the pellets were dissolved in 0.01 M phosphate buffer at pH 7.5. After centrifugation at 4 °C, 5,000*g* for 10 min, the supernatant was further centrifuged at 4 °C, 100,000*g* for 2 h. The resulting pellets were dissolved in 0.01 M phosphate buffer

at pH 7.5. Carefully laid the resuspended pellet solution on top of 20% glycerol cushion. The virus particles were pelleted by centrifugation at 4 °C, 100,000*g* for 2 h. After centrifugation, discarded the supernatant and dissolved the pellets in 0.01 M phosphate buffer at pH 7.5. The purified virus particles were characterized by 10% SDS–PAGE, and the virus concentration was determined using the Bradford assay with BSA as a standard. The purified particles were then stored at −80 °C. When conducting rice protoplast infection, 1 μg RSV particles, 10 μg corresponding plasmid and 110 μl freshly prepared PEG-$CaCl_2$ solution were gently mixed with 100 μl of protoplasts and then incubated for 15 min at room temperature in the dark. After transfection, the cells were washed with 10 volumes of W5 and then resuspended in W1 solution overnight at 28 °C in the dark. The infected protoplasts were collected at 18 h after infection and the RSV RNAs and RSV CP accumulation were analysed using RT–qPCR and immunoblotting.

Protein expression and ubiquitination assay in *E. coli*

The protein expression and ubiquitination assays conducted in the *E. coli* strain BL21 (DE3) were performed according to previous studies[42]. In brief, different combinations of the indicated expression vectors were transformed into the *E. coli* strain BL21 (DE3), and the strains were cultured in Luria–Bertani liquid medium at 37 °C. Then, 0.5 mM IPTG was added to the medium when the absorbance at 600 nm reached 0.4–0.6 to induce the expression of the target proteins. The bacteria were further cultured at 28 °C for 10–12 h and then stored at 4 °C overnight. The crude proteins were extracted and analysed by western blotting with the corresponding antibodies.

MST assay

The MST assays were conducted as previously described[17]. To assess the binding affinity between OsRBRL and RSV CP or RDV P2, we first labelled the GST–CP and MBP–$P2^{1–786}$ protein with the red fluorescent dye NHS according to the instructions of the Monolith Series Protein Labeling Kit RED-NHS 2nd Generation (NanoTemper Technologies). The NHS-labelled GST–CP and MBP–$P2^{1–786}$ protein was gradually diluted until its fluorescence intensity ranged between 800 and 1,000 under 20% LED power. The initial concentration of the MBP–OsRBRL protein was 258 μM. It was subjected to 12 rounds of 1:1 serial dilution to a final concentration of 0.126 μM. After brief incubation in the dark, the samples were loaded into MST standard capillaries. The measurements were performed with 20% MST power on a Microscale Thermophoresis Monolith NT.115 instrument (NanoTemper Technologies). The assays were repeated at least twice for each affinity measurement. Data analyses were performed using the MO.Affinity analysis software provided by the manufacturer.

Transcriptome sequencing

The aboveground parts of the mock- and RSV-infected rice plants were collected at 4 w.p.i. The plant material was thoroughly ground in liquid nitrogen and approximately 0.1 g of the sample was used for RNA extraction (see the 'RNA extraction and RT–qPCR analysis' section). Library construction and paired-end RNA-seq were performed by Biomarker Technologies. FastQC software was used to assess the quality of the raw sequencing reads. After adapters and low-quality reads were removed, the clean reads were mapped to the rice genome (MSU Rice Genome Annotation Project Database v.7.0, https://rice.uga.edu/download_osa1r7.shtml) using TopHat. Gene expression levels were calculated as fragments per kilobase per million reads. The multiple-testing-adjusted *P* value (false-discovery rate < 0.01) with an absolute fold change ≥ 2 was used to determine whether individual genes were significantly differentially expressed.

RBRL nuclear exclusion experiments

We conducted an RBRL nuclear-export experiment based on those performed in previous studies[72]. To prevent RBRL from localizing within the nucleus, a NES corresponding to amino acids 371 to 387 of *Arabidopsis thaliana* RTL2 (KKAESSSAYHMIRALRK) was introduced into the vector Ubi::RBRL-GFP. After sequencing verification, the modified construct was transformed into rice protoplasts with RSV particles (see the 'Transient expression in rice protoplasts' and 'Virus isolation and rice protoplast infection' sections).

Proteasome assembly assay

The proteasome assembly assays were conducted as previously described[73]. The aboveground parts of the mock- and RSV-infected NPB plants were collected at 4 w.p.i. The total protein extracted with buffer F (50 mM Tris-HCl (pH 7.5), 25 mM NaCl, 2 mM $MgCl_2$, 1 mM EDTA, 2 mM DTT, 5 mM ATP and 5% glycerol) was used for native PAGE, followed by standard western blotting. Proteasome extracted from one-month-old *A. thaliana* Col-0 ecotype were used as a positive control and the marker. The anti-PAG1 antibody (1:1,000)[73] was used to detect the assembly of proteasome.

Histochemical staining of H_2O_2 and $O_2^{\cdot-}$

Hydrogen peroxide (H_2O_2) and superoxide ($O_2^{\cdot-}$) in rice leaves were detected using the 3,3′-diaminobenzidine (DAB, Sigma-Aldrich) and nitro blue tetrazolium (NBT, Sigma-Aldrich) staining methods, with minor modifications based on previously described protocols[19]. In brief, rice leaves approximately 1 cm in length were immersed in either 10 mM Tris-HCl buffer (pH 6.5) containing DAB (1 mg ml^{-1}) for H_2O_2 detection or 50 mM sodium phosphate buffer (pH 7.0) containing NBT (0.05%) for $O_2^{\cdot-}$ detection. The samples were incubated in the dark at 37 °C for 16 h. After incubation, the leaves were bleached with a solution of ethanol and acetic acid (3:1) at 70 °C for 60 min to remove chlorophyll. Finally, the leaves were washed 4–5 times with 75% ethanol until clear and photographed through a stereomicroscope under uniform lighting conditions.

H_2O_2 determination in rice seedlings

To quantify H_2O_2 levels in rice seedlings, a standardized protocol was used. Fresh rice leaves (100 mg) were weighed and ground into a fine powder using liquid nitrogen. The powder was mixed with 1 ml of 50 mM sodium phosphate buffer (pH 7.4) and incubated on ice for 30 min to facilitate H_2O_2 extraction. After incubation, the mixture was centrifuged at 13,000 rpm for 10 min at 4 °C and the supernatant was carefully transferred to a new tube. The H_2O_2 concentration was then determined using the Amplex Red Hydrogen Peroxide/Peroxidase Assay Kit (Invitrogen, A22188) according to the manufacturer's instructions. The absorbance was measured at approximately 560 nm using a BioTek Microplate Reader (BioTek Cytation5), and the H_2O_2 content was calculated by comparing the sample absorbance to a standard curve of known H_2O_2 concentrations.

Quantification and statistical analysis

The data from the JA quantitative assays were analysed using two-way ANOVA. The data from the RT–qPCR analysis, dual-luciferase reporter system and protein degradation assay were analysed using Student's *t*-tests or one-way ANOVA with Tukey's multiple-comparison test. The above statistical analyses were performed with GraphPad Prism (v.7.0). All descriptive statistics of the JA quantitative analysis, RT–qPCR analysis, dual-luciferase reporter system and RSV disease symptom classification are shown as the mean ± s.d. The number (*n*) of biological replicates is indicated in each legend. For immunoblotting quantification, the band intensities were quantified using ImageJ. No statistical method was used to predetermine sample size. The sample sizes were determined from experimental trials and previous publications on similar experiments. Blinding and randomization were used. For example, the virus-infection assay, different rice lines were numbered; the investigator was blinded to the group allocation during the experiments including the inoculation of

viruliferous small brown planthopper, the infection rates statistics, and virus RNAs RT–qPCR analysis. All samples were arranged randomly into experimental groups. Plants for experiments were grown side by side to minimize unexpected environmental variations during growth.

Statistics and reproducibility

Statistical analyses in Fig. 2g and Extended Data Figs. 3d,e and 4d were performed using one-way ANOVA with Tukey's multiple-comparison tests, and different letters represent significantly different groups at the $P < 0.05$ level. Owing to the large number of P values obtained from pairwise comparisons, we list the exact P values in the corresponding source data as part of the Supplementary Information.

Material availability

All materials needed to replicate the work are available.

Reporting summary

Further information on research design is available in the Nature Portfolio Reporting Summary linked to this article.

Data availability

OsRBRL (LOC_Os03g42760), *OsRBRL-like* (LOC_Os03g42780), *OsNINJA1* (LOC_Os03g11550), *OsNINJA2* (LOC_Os07g41160), *OsNINJA3* (LOC_Os03g30570) and *OsNINJA4* (LOC_Os05g48500) are available from the Rice Genome Annotation Project Database (https://rice.uga.edu/). RNA-seq raw data have been deposited at the Genome Sequence Archive in National Genomics Data Center, China National Center for Bioinformation/Beijing Institute of Genomics, Chinese Academy of Sciences (CRA020855) and are publicly accessible. Uncropped immunoblotting images are provided in Supplementary Fig. 1. Source data are provided with this paper.

59. Yang, D.-L. et al. Plant hormone jasmonate prioritizes defense over growth by interfering with gibberellin signaling cascade. *Proc. Natl Acad. Sci. USA* **109**, E1193 (2012).
60. Miao, J. et al. Targeted mutagenesis in rice using CRISPR-Cas system. *Cell Res.* **23**, 1233–1236 (2013).
61. Fu, S. et al. Rice stripe virus interferes with *S*-acylation of remorin and induces its autophagic degradation to facilitate virus infection. *Mol. Plant* **11**, 269–287 (2018).
62. Jin, L. et al. Rice dwarf virus P2 protein hijacks auxin signaling by directly targeting the rice OsIAA10 protein, enhancing viral infection and disease development. *PLoS Pathog.* **12**, e1005847 (2016).
63. Liu, C. et al. *Arabidopsis* ARGONAUTE 1 binds chromatin to promote gene transcription in response to hormones and stresses. *Dev. Cell* **44**, 348–361 (2018).
64. Yu, F. et al. ESCRT-I component VPS23A is targeted by E3 ubiquitin ligase XBAT35 for proteasome-mediated degradation in modulating ABA signaling. *Mol. Plant* **13**, 1556–1569 (2020).
65. Pan, W. et al. The UBC27–AIRP3 ubiquitination complex modulates ABA signaling by promoting the degradation of ABI1 in *Arabidopsis*. *Proc. Natl Acad. Sci. USA* **117**, 27694–27702 (2020).
66. Liu, L. et al. An efficient system to detect protein ubiquitination by agroinfiltration in *Nicotiana benthamiana*. *Plant J.* **61**, 893–903 (2010).
67. Yao, S. et al. The key micronutrient copper orchestrates broad-spectrum virus resistance in rice. *Sci. Adv.* **8**, eabm0660 (2022).
68. Forcat, S., Bennett, M. H., Mansfield, J. W. & Grant, M. R. A rapid and robust method for simultaneously measuring changes in the phytohormones ABA, JA and SA in plants following biotic and abiotic stress. *Plant Methods* **4**, 16 (2008).
69. Yang, R. et al. Fine-tuning of miR528 accumulation modulates flowering time in rice. *Mol. Plant* **12**, 1103–1113 (2019).
70. Yao, S. et al. Transcriptional regulation of miR528 by OsSPL9 orchestrates antiviral response in rice. *Mol. Plant* **12**, 1114–1122 (2019).
71. Wang, Y. et al. Molecular variation in a functionally divergent homolog of FCA regulates flowering time in *Arabidopsis thaliana*. *Nat. Commun.* **11**, 5830 (2020).
72. Muñoz-Díaz, E. & Sáez-Vásquez, J. Nuclear dynamics: formation of bodies and trafficking in plant nuclei. *Front. Plant Sci.* **13**, 984163 (2022).
73. Han, J. et al. The β5 subunit is essential for intact 26S proteasome assembly to specifically promote plant autotrophic growth under salt stress. *N. Phytol.* **221**, 1359–1368 (2019).

Acknowledgements We thank D. Xie, C. Li, Y. Ning, J. Zhou, W. Wang, S. Ding and F. Qu for their insights and suggestions; Z. He for providing the *coi1-13* seeds used in this study; D. Lu for supplying the Duet expression vectors used to reconstitute the plant ubiquitination cascade in *E. coli*; F. Qin for supplying the pGreenII vectors used in this study; X. Zhou, J. Wu and F. Cui for providing the RSV CP antibody used in this study; L. Xiong for providing the rice seeds of the *ninja1* T-DNA mutants and wild-type DJ; the staff at the National Center for Protein Sciences and the Core Facilities at the School of Life Sciences at Peking University for their support with the MS experiments and UPLC–MS/MS procedures. We acknowledge the contributions of the staff at HUABIO (Hangzhou, China) and ABclonal Biotechnology (Wuhan, China) to generating the antibodies used in this research. Financial support for this study was provided by the Ministry of Science and Technology (2021YFA1300702) and the Natural Science Foundation of China (31530062 and 32090010).

Author contributions Y. Huang, J.Y., Z.Y. and Y.L. designed the experiments. Y. Huang, J.Y., Z.Y. and X.S. performed most of the experiments. J.L., L.D., S.L., Y.J. and T.Z. helped conducting virus inoculation assays. H.W. helped with rice plant cultivation and seed multiplication. J.-j.H. helped with conducting proteasome assembly assays. Z.Y., Y.L., X.C., S.Y., Y. Han, C.C. and Q.X. contributed to experimental data analysis. Y. Huang, J.Y., Z.Y. and Y.L. wrote the manuscript. Y. Huang, J.Y., X.S., W.W., C.W., Q.X., Z.Y. and Y.L. revised the manuscript. All of the authors discussed the results and commented on the manuscript.

Competing interests The authors declare no competing interests.

Additional information

Supplementary information The online version contains supplementary material available at https://doi.org/10.1038/s41586-025-08706-8.

Correspondence and requests for materials should be addressed to Zhirui Yang or Yi Li.

Peer review information *Nature* thanks Alain Goossens, Zuhua He and the other, anonymous, reviewer(s) for their contribution to the peer review of this work. Peer reviewer reports are available.

a

Sample	Protein	Score	Intensity
CP-OE	CP	38.10	7.38×10^{6}
	RBRL	11.87	1.59×10^{6}
RSV-infected NPB	CP	323.31	1.11×10^{9}
	RBRL	6.15	2.40×10^{6}

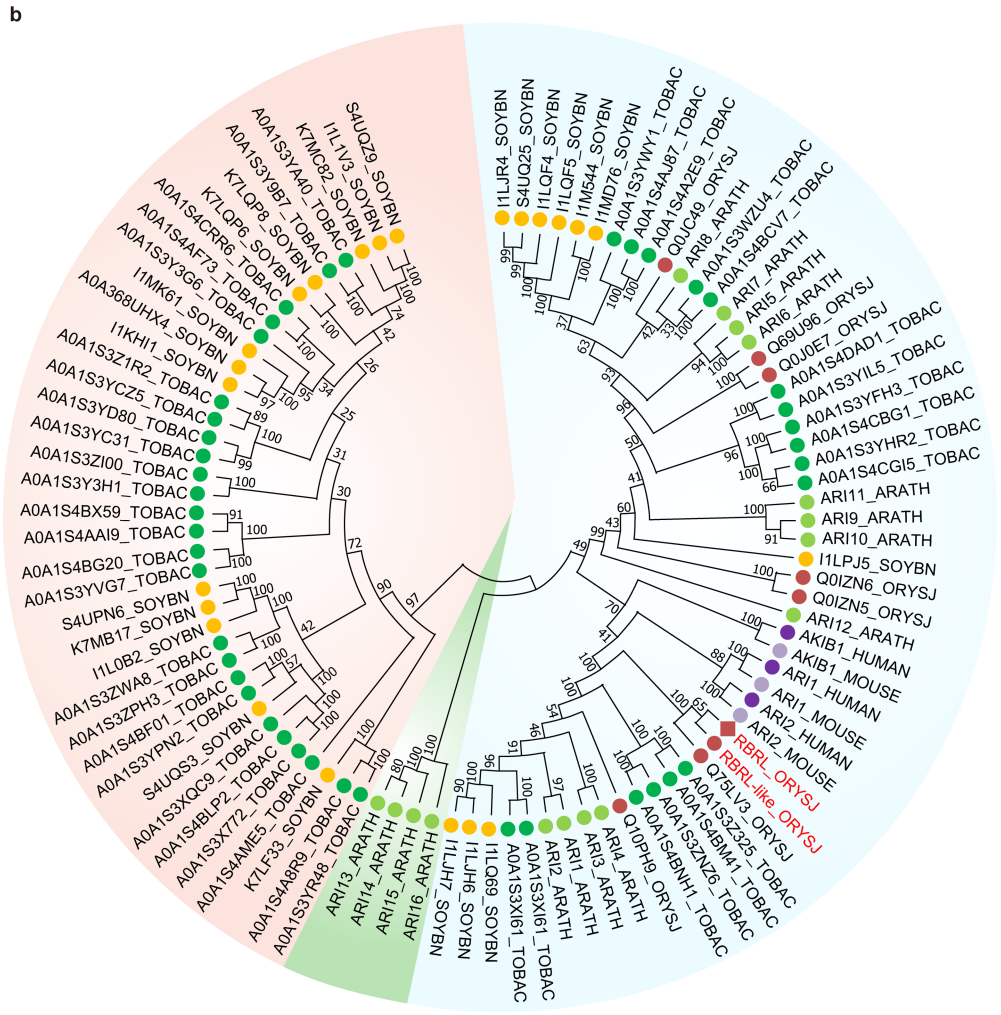

Extended Data Fig. 1 | See next page for caption.

Extended Data Fig. 1 | Phylogenetic analysis of RBR-type E3 ligases. a, Scores and intensities of the CP protein and its interacting protein RBRL identified by mass spectrometry in different samples. **b**, Phylogenetic analysis of RBR-type E3 ligases in rice and other species. An unrooted, neighbour-joining tree was constructed by aligning RBR-type E3 ligase sequences from rice and other species. The proteins are colour-coded dark red for rice (*Oryza sativa*), yellow for soybean (*Glycine max*), light green for Arabidopsis (*Arabidopsis thaliana*), dark green for tobacco (*Nicotiana tabacum*), light purple for mouse (*Mus musculus*) and dark purple for human (*Homo sapiens*). Rice OsRBRL (RBRL_ORYSJ) and its homologue, OsRBRL-like protein (RBRL-like_ORYSJ), are highlighted in red. **c**, Sequence alignment of OsRBRL and OsRBRL-like proteins. The RING1, IBR, RING2, and Ariadne domains are indicated by horizontal lines. **d**, Expression analysis of *OsRBRL* and *OsRBRL-like* via transcriptome sequencing (RNA-seq) data. FPKM, fragments per kilobase of exon per million reads mapped. Statistical analysis was performed via two-sided Student's *t* tests, and all *p* values are shown in the figure. The data are the mean ± s.d. $n = 3$ independent biological samples.

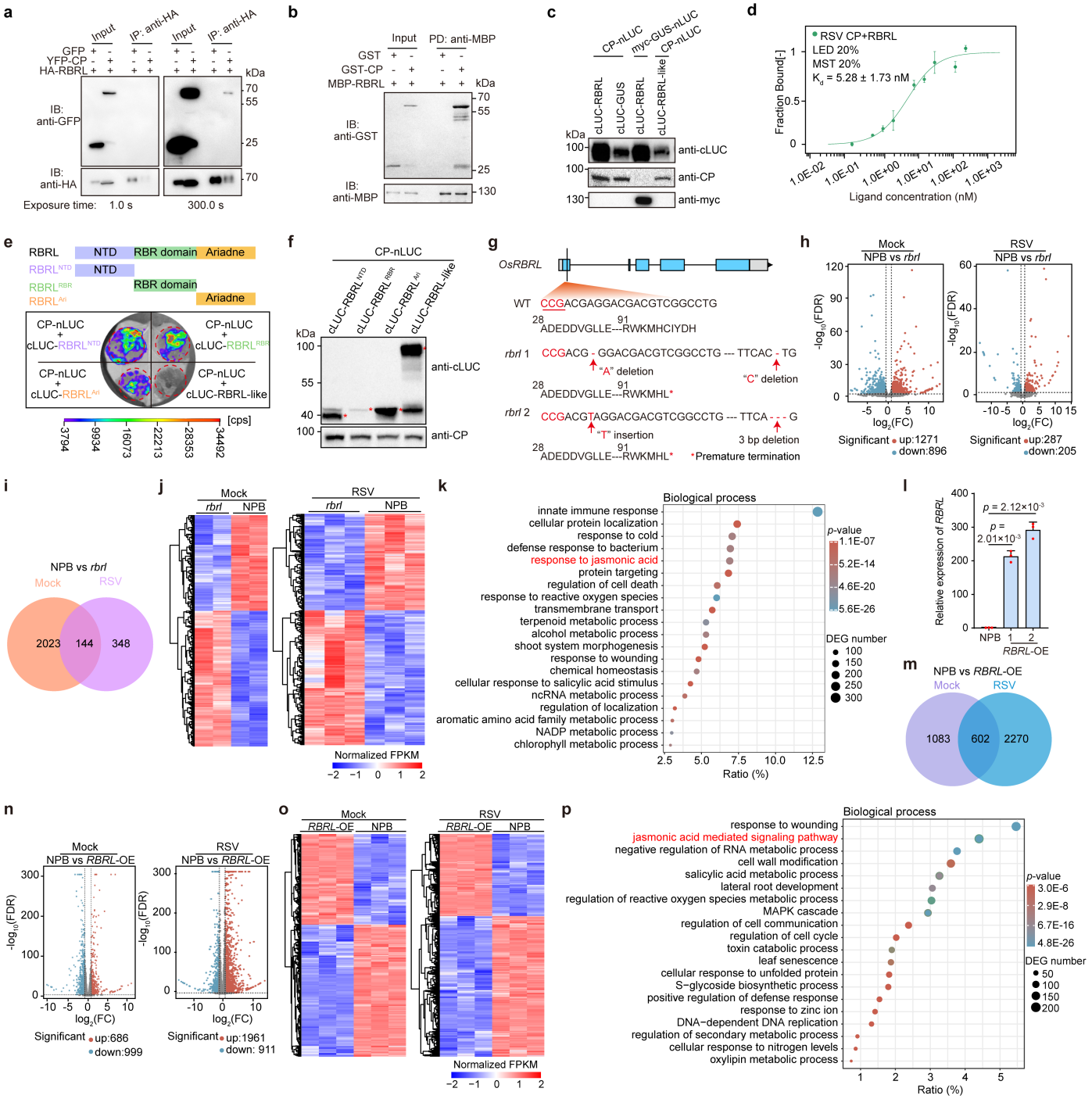

Extended Data Fig. 2 | See next page for caption.

Extended Data Fig. 2 | OsRBRL interacts with RSV CP and plays a role in JA signalling pathway. a, Co-IP assays of YFP-CP and HA-RBRL revealed that RSV CP interacts with OsRBRL in *N. benthamiana* leaves. GFP was used as a negative control. IP, immunoprecipitation. IB, immunoblotting. **b**, In vitro pull-down assays illustrating the interaction between RSV CP and OsRBRL. GST served as a negative control. PD, pull-down. **c**, Protein detection of different transient expression combinations in the LCI assays (Fig. 1d). The indicated proteins were detected via the corresponding antibodies. **d**, MST assays showing the binding affinity between RSV CP and OsRBRL. The data are the mean ± s.d. $n = 3$ independent biological samples. **e**, LCI assays showing that the RSV CP interacts with the N-terminal domain (NTD), RBR domain, and Ariadne domain of OsRBRL. cLUC-RBRL-like served as a negative control. cps, signal counts per second. **f**, Protein detection of different transient expression combinations in the LCI assays **(e)**. The indicated proteins were detected via the corresponding antibodies. The red asterisks indicate the target protein bands. The analyses in **a-c** and **f** were repeated two to three times with similar results. **g**, Generation of *rbrl*-knockout (CRISPR/Cas9) lines. The guide RNA (gRNA) sequence targeting *OsRBRL* is indicated, and the protospacer-adjacent motif (PAM) is highlighted in red. In *rbrl* line, an 'A' deletion and a 'C' deletion in the gRNA target site resulted in premature translational termination of *OsRBRL*. In *rbrl* line 2, a 'T' insertion and a 3-bp deletion in the gRNA target site resulted in premature termination of the translation of *OsRBRL*. **h**, Volcano plots representing the fold changes in the expression of differentially expressed genes (DEGs) in the NPB versus *rbrl* comparisons with or without the virus (FDR < 0.01, fold change ≥ 2.0). **i**, Venn diagram representing DEGs regulated by *OsRBRL*. **j**, Hierarchical clustered heatmap of 2167 DEGs (1271 upregulated genes and 896 downregulated genes, left) and 492 DEGs (287 upregulated genes and 205 downregulated genes, right). **k**, Gene Ontology (GO) analysis showing 20 representative enrichment terms of all the DEGs shown in (**i**). The significance of the GO terms was using adjusted $p < 0.05$ (Fisher's exact test). **l**, RT–qPCR analysis of the *OsRBRL* expression level in the NPB and *RBRL*-OE plants. Statistical analysis was performed via two-sided Student's *t* tests, and all *p* values are shown in the figure. The data are the mean ± s.d. $n = 3$ independent biological samples. **m**, Venn diagram representing DEGs regulated by *OsRBRL*. **n**, Volcano plots representing the fold change in expression of the DEGs in the NPB versus *RBRL*-OE comparisons with or without the virus (FDR < 0.01, fold change ≥ 2.0). **o**, Hierarchical clustered heatmap of 1685 DEGs (686 upregulated genes and 999 downregulated genes, left) and 2872 DEGs (1961 upregulated genes and 911 downregulated genes, right). **p**, GO analysis showing 20 representative enrichment terms of all the DEGs shown in (**m**). The significance of the GO terms was using adjusted $p < 0.05$ (Fisher's exact test).

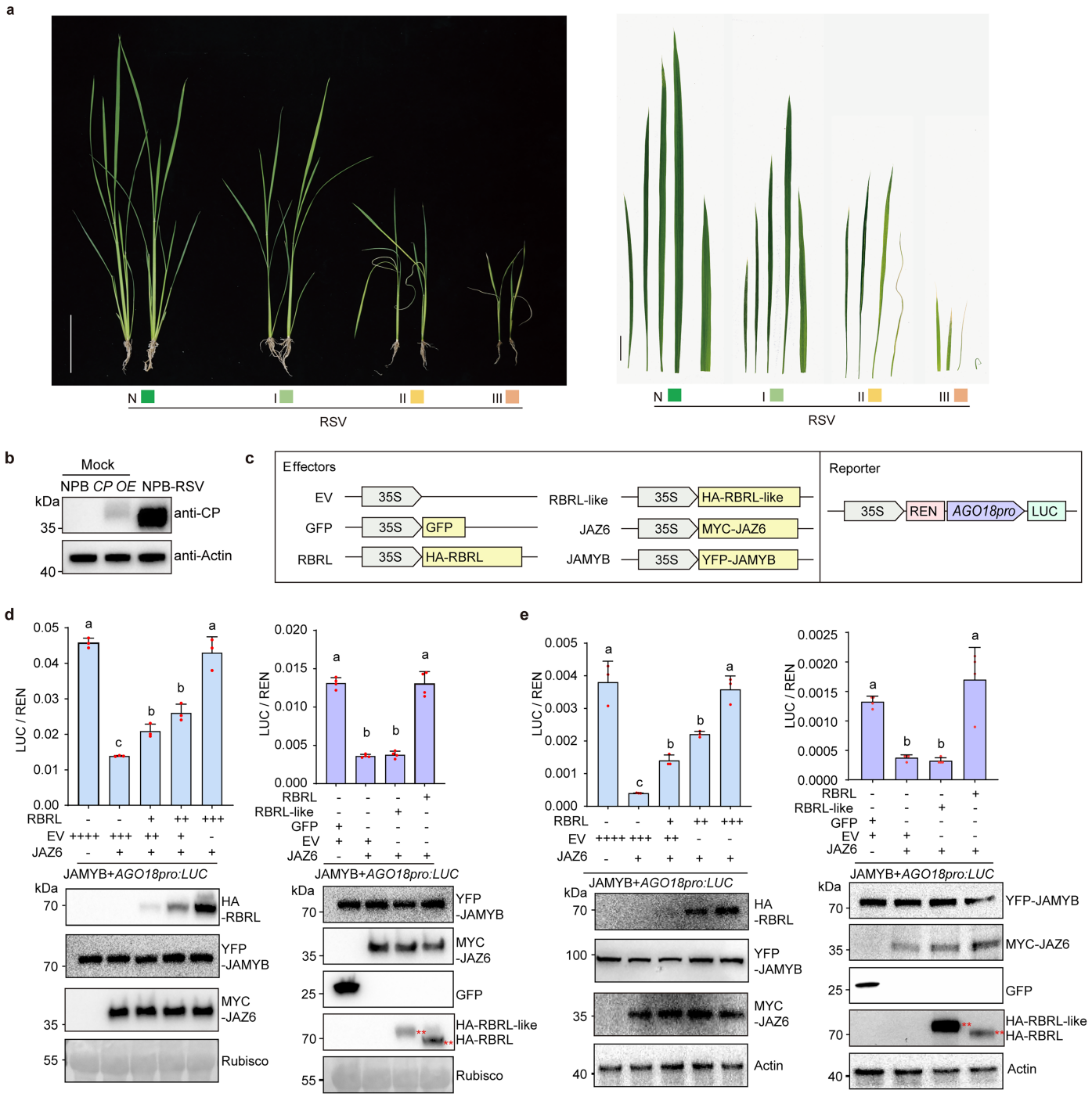

Extended Data Fig. 3 | OsRBRL promotes the transcription of *OsAGO18* in *N. benthamiana* leaves and rice protoplasts. a, Photographs of RSV-infected NPB plants with different degrees of disease symptoms. The photographs were taken at 4 w.p.i. Scale bars, 10 cm (left panel) and 2 cm (right panel). N, no noticeable symptoms; I, mild symptoms on the fourth or fifth leaf; II, typical yellow stripes on the third leaf and curl or death of the fourth leaf; III, curl or death of the third leaf. **b**, Immunoblotting analysis of the RSV CP levels in the specified plants. All the mock-inoculated rice plants were 6-week-old and all the RSV-infected plants were collected at 4 w.p.i. Actin served as sample processing controls. The analysis was repeated four times with similar results. **c**-**e**, Dual-luciferase assays in *N. benthamiana* leaves **(d)** and rice protoplasts **(e)**. A schematic diagram of the constructs is shown in **(c)**. EV: empty vector. The activities of firefly luciferase (LUC) and Renilla luciferase (REN) were measured sequentially, and the LUC/REN ratio was calculated as the final transcriptional activity. The data are the mean ± s.d. $n = 3$ (left panels in **d** and **e**) or 4 (right panels in **d** and **e**) independent biological samples. Statistical analysis was performed via one-way analysis of variance (ANOVA) with Tukey's multiple comparison test (different letters represent significantly different groups; $p < 0.05$). Immunoblotting analysis of all the proteins in the corresponding dual-luciferase assays were shown in the lower panels. Rubisco and Actin served as sample processing controls.

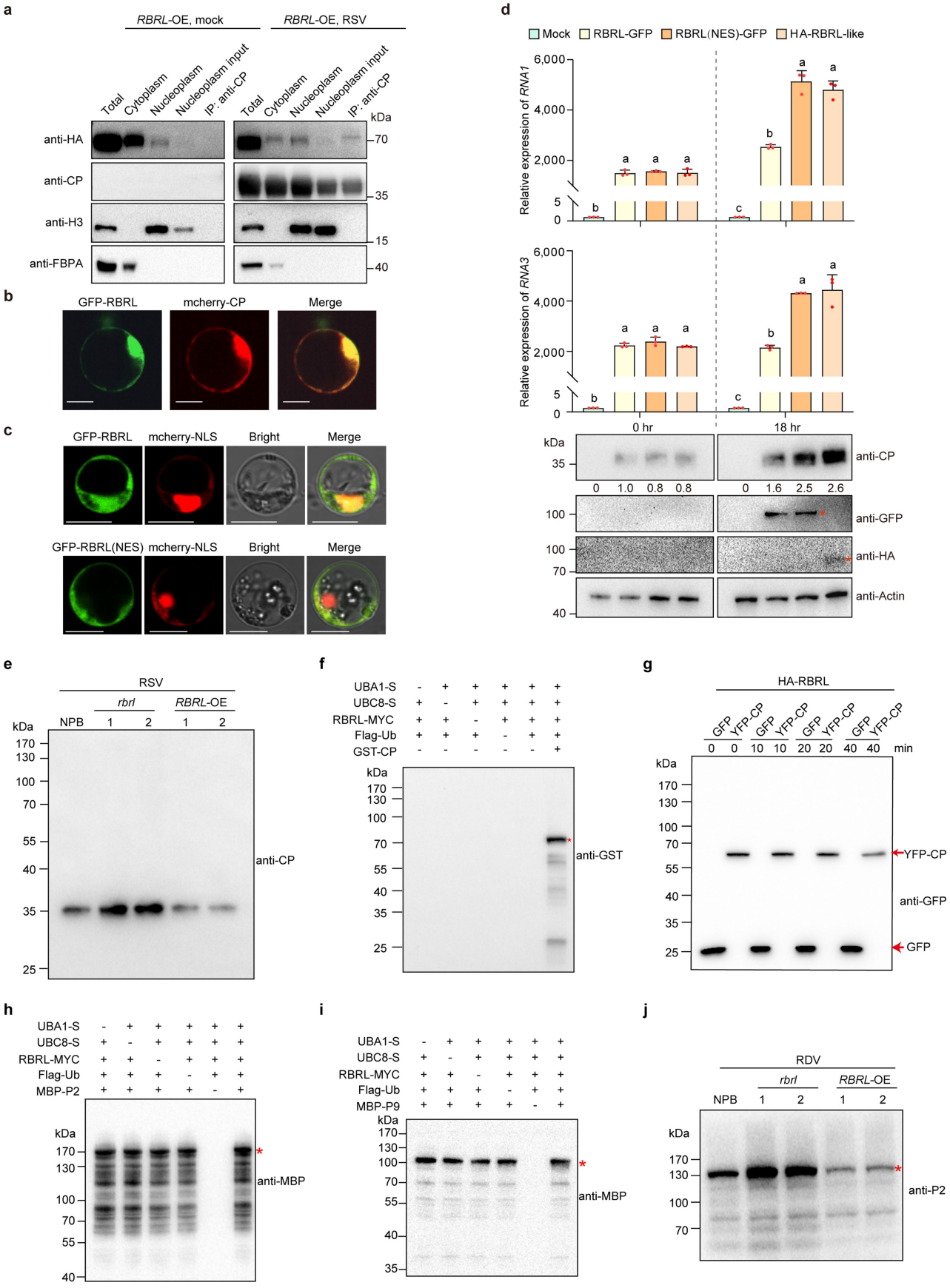

Extended Data Fig. 4 | See next page for caption.

Extended Data Fig. 4 | OsRBRL colocalizes with CP in rice, and its biological function depends on its nuclear localization, but OsRBRL does not ubiquitinate viral coat proteins. a, IP assays were conducted with the nuclear fraction of mock-inoculated and RSV-infected *RBRL*-OE plants. FBPA served as a cytoplasmic marker, and histone H3 served as a nuclear marker. Mock-inoculated *RBRL*-OE plants served as a negative control. **b**, Subcellular localization of GFP-RBRL and mCherry-CP in rice protoplasts. Scale bars, 10 μm. **c**, RBRL(NES) was observed to be localized in the cytoplasm via confocal microscopy. scale bars, 10 μm. **d**, RT–qPCR analysis (upper panel) of RSV RNAs accumulation in the rice protoplast transfected with *RBRL-GFP*, *RBRL(NES)-GFP* or *HA-RBRL-like*, together with RSV. Immunoblotting analysis (lower panel) of RSV CP accumulation, RBRL-GFP, RBRL(NES)-GFP and HA-RBRL-like expression in the indicated samples. Actin served as loading controls. Mock, the protoplasts did not transfect with RSV. Data are shown as mean ± s.d. $n = 3$ independent biological samples. Statistical analysis was performed via one-way analysis of variance (ANOVA) with Tukey's multiple comparison test (different letters represent significantly different groups; $p < 0.05$). **e**, Full gel graph of the immunoblotting analysis of CP in the indicated plants; no ubiquitinated bands of CP were detected. **f**. Full gel graph of the immunoblotting analysis of CP in the bacterial ubiquitination system (related to Fig. 3e). **g**. Full gel graph of the immunoblotting analysis of CP in the semi-in vivo degradation experiments (related to Fig. 3f). **h**, Ubiquitination analysis of P2 by RBRL. Bacterial lysates from *E. coli* strains expressing UBA1-S (E1), UBC8-S (E2), Flag-Ub, MBP-P2 and RBRL-MYC or from strains lacking one of these components were analysed by immunoblotting with an anti-MBP antibody to determine the expression of P2. **i**, Ubiquitination analysis of P9 by RBRL. Bacterial lysates from *E. coli* strains expressing UBA1-S (E1), UBC8-S (E2), Flag-Ub, MBP-P9 and RBRL-MYC or from strains lacking one of these components were analysed by immunoblotting with an anti-MBP antibody to determine the expression of P9. **j**, Full gel graph of the immunoblotting analysis of RDV P2 levels in the indicated plants; no ubiquitinated bands of P2 were detected (related to Extended Data Fig. 10l). All the experiments were repeated two to four times with similar results.

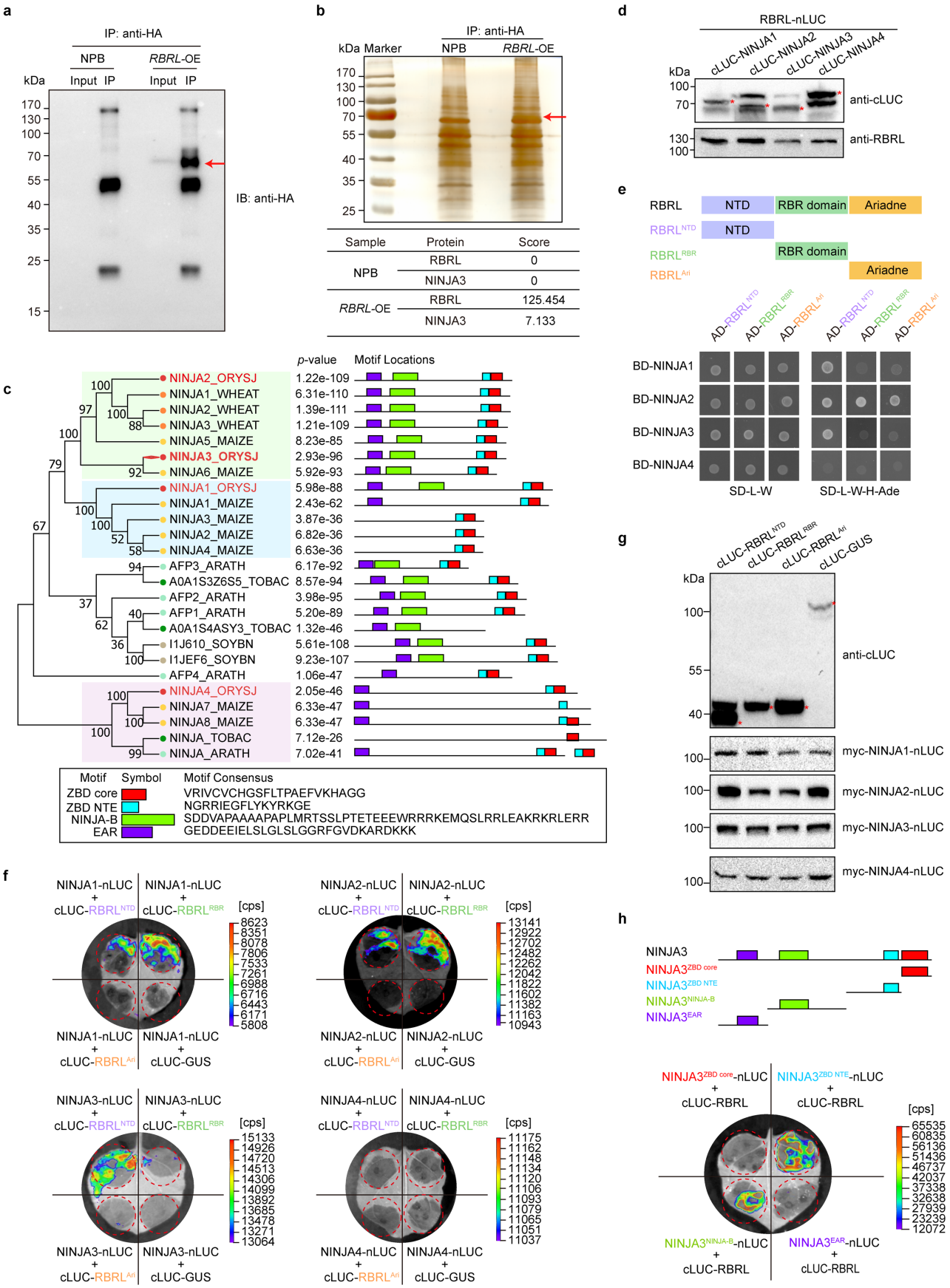

Extended Data Fig. 5 | See next page for caption.

Extended Data Fig. 5 | Identification of potential substrates of OsRBRL and functional domains involved in the interaction between OsRBRL and OsNINJA3. a-b, HA-RBRL and its interaction proteins purified with anti-HA magnetic agarose from proteins extracts of *RBRL*-OE rice lines were detected by immunoblotting with anti-HA antibody (**a**) and silver staining (**b**). OsRBRL expressed in *RBRL*-OE lines was labelled with a 1× HA tag at the N-terminus. Wild-type NPB plants served as the negative control. Red arrows indicate the specific RBRL band. Scores of the RBRL protein and its interacting protein NINJA3 identified by mass spectrometry in different samples. **c**, Phylogenetic analysis was conducted using the full-length protein sequences of OsNINJA3 and NINJA family proteins from the indicated plant species. The proteins are colour-coded red for rice (*Oryza sativa* subsp. japonica), orange for wheat (*Triticum aestivum*), yellow for maize (*Zea mays*), light green for Arabidopsis (*Arabidopsis thaliana*), dark green for tobacco (*Nicotiana tabacum*), and grey for soybean (*Glycine max*). Rice NINJA proteins are highlighted in red. Conserved motif analysis was performed via the online software program MEME (http://meme-suite.org/tools/meme). **d**, Protein detection of different transient expression combinations in the LCI assays (Fig. 4b). The indicated proteins were detected via the corresponding antibodies. The red asterisks indicate the target protein bands. **e**, Y2H assays showing that the N-terminal domain (NTD) of OsRBRL primarily interacts with OsNINJA1/2/3. OsNINJA4 served as a negative control. **f**, LCI assays showing that the N-terminal domain (NTD) of OsRBRL primarily interacts with OsNINJA1/2/3. cLUC-GUS served as a negative control. cps, signal counts per second. **g**, Protein detection of different transient expression combinations in the LCI assays **(f)**. The indicated proteins were detected via the corresponding antibodies. The red asterisks indicate the target protein bands. The analyses in **a**, **b**, **d** and **g** were repeated at least two times with similar results. **h**, LCI assays showing that the NINJA-B and ZBD NTE regions but not the EAR motif of OsNINJA3 interact with OsRBRL. cps, signal counts per second.

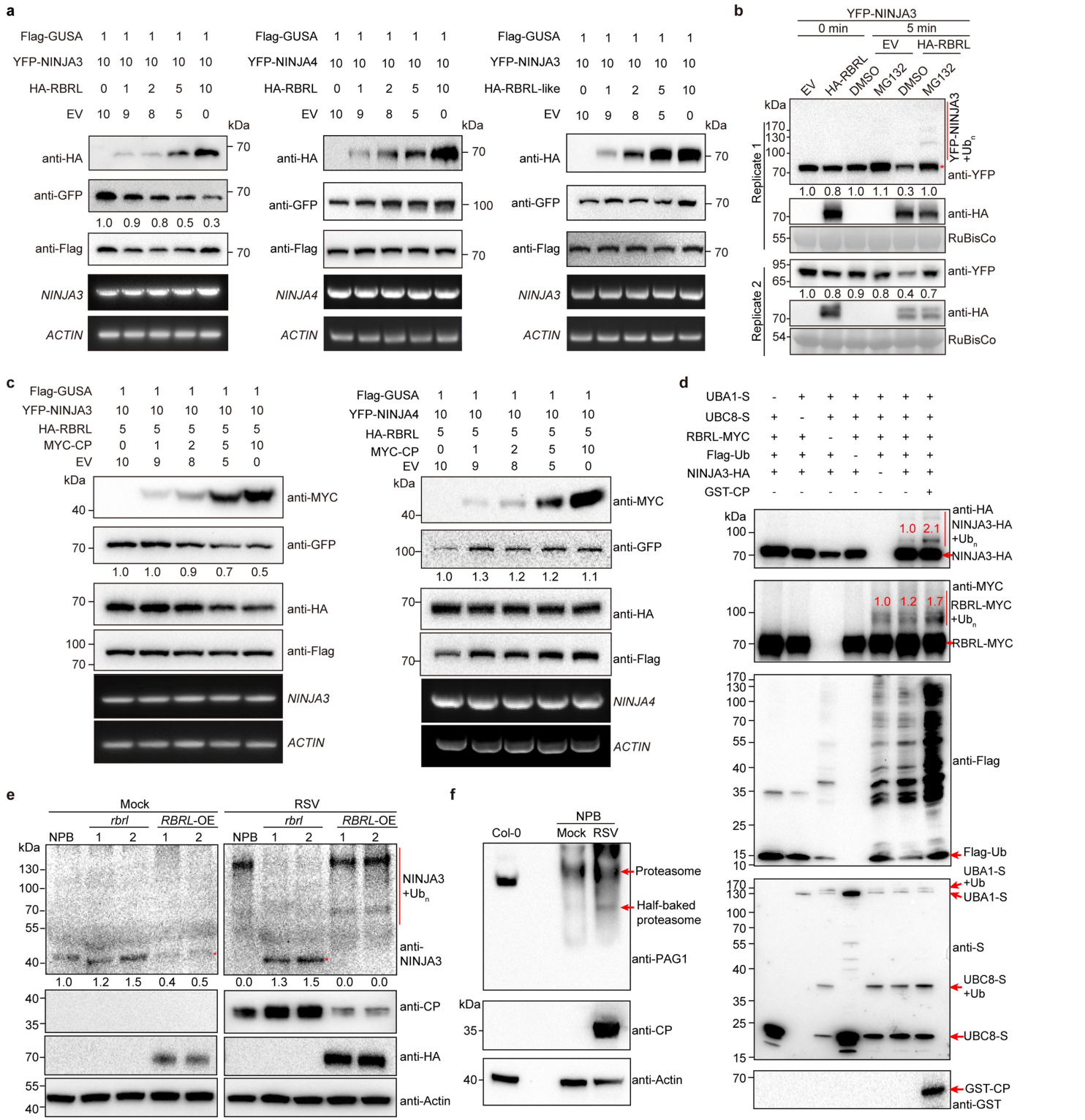

Extended Data Fig. 6 | See next page for caption.

Extended Data Fig. 6 | OsRBRL mediates the degradation of OsNINJA3 through the 26S proteasome. a, The in vivo degradation of NINJA3 was assessed by determining the YFP-NINJA3 protein level via co-infiltration experiments with increasing amounts of HA-RBRL. Flag-GUSA served as the internal control. The mRNA levels of *ACTIN*, *NINJA3* and *NINJA4* were analysed via reverse transcriptase–polymerase chain reaction (RT–PCR) to ensure that equal amounts of *NINJA3* or *NINJA4* were transcribed across the co-infiltration conditions. The numbers at the top denote the ratios of the concentrations of *Agrobacterium* used for co-infiltration. YFP-NINJA4 (middle panel) and HA-RBRL-like (right panel) served as negative controls. **b**, Effect of the proteasome inhibitor MG132 on OsNINJA3 degradation by OsRBRL. MG132 was added to the corresponding protein mixture samples at a final concentration of 50 μM to prevent protein degradation through the 26S proteasome. Dimethyl sulfoxide (DMSO) was used as a control. Ponceau S staining of the Rubisco proteins served as sample processing controls. **c**, The in vivo degradation of OsNINJA3 was conducted by determining the YFP-NINJA3 protein level via co-infiltration experiments with increasing amounts of MYC-CP. Flag-GUSA was used as the internal control. The mRNA expression levels of the target genes *OsNINJA3* and *ACTIN* were analysed via RT–PCR. The numbers at the top indicate the ratio of the concentrations of *Agrobacterium* used in co-infiltration. YFP-NINJA4 (right panel) served as a negative control. **d**, CP promotes the ubiquitination of NINJA3 by OsRBRL. The bacterial lysates from *E. coli* strains expressing UBA1-S, UBC8-S, Flag-Ub, RBRL-MYC, MBP-NINJA3-HA and GST-CP or from strains lacking one of these components were analysed by immunoblotting with an anti-HA antibody to detect the ubiquitination of OsNINJA3. **e**, Immunoblotting analysis of OsNINJA3 levels in the plants indicated by the asterisk. The red line denotes the ubiquitinated form of NINJA3. Actin served as sample processing controls. **f**, Proteasome assembly in mock-treated and RSV-infected NPB plants were detected with anti-PAG1 antibody via native polyacrylamide gel electrophoresis (PAGE). Arabidopsis (Col-0 ecotype) proteasome was also detected as a positive control and the marker. Proteasome and half-baked proteasome are indicated. Actin was used as the loading control. All the experiments were repeated two to four times with similar results.

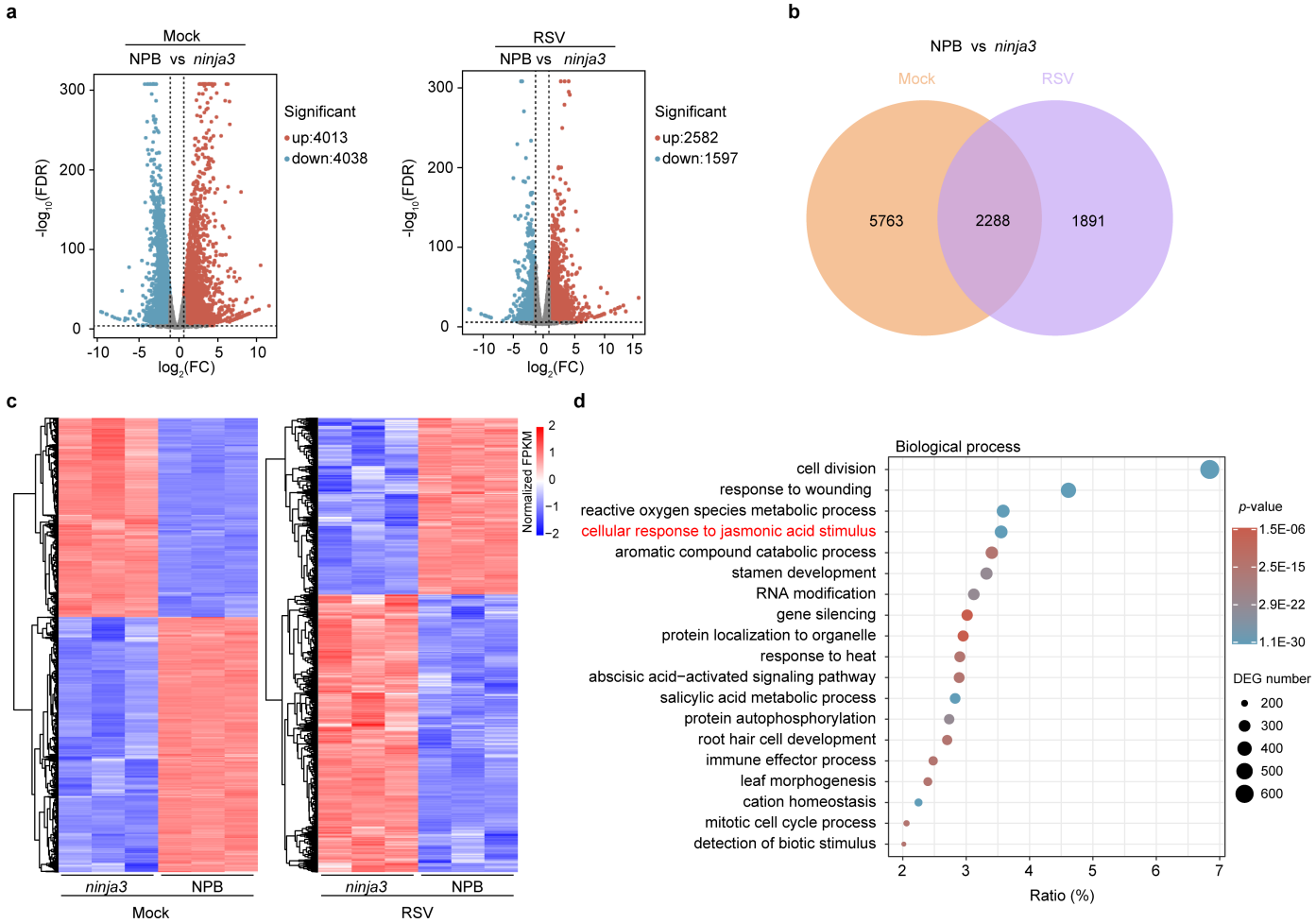

Extended Data Fig. 7 | Transcriptome analysis of NPB and *ninja3* with or without RSV infection. a, Volcano plots representing the fold change in the expression of the DEGs in the NPB versus *ninja3* comparisons with or without the virus (FDR < 0.01, fold change ≥ 2.0). **b**, Venn diagram representing DEGs regulated by OsNINJA3. **c**, Hierarchical clustered heatmap of 8051 DEGs (4013 upregulated genes and 4038 downregulated genes, left) and 4179 DEGs (2582 upregulated genes and 1597 downregulated genes, right). **d**, GO analysis showing 19 representative enrichment terms of all the DEGs shown in (**b**). The significance of the GO terms was using adjusted $p < 0.05$ (Fisher's exact test).

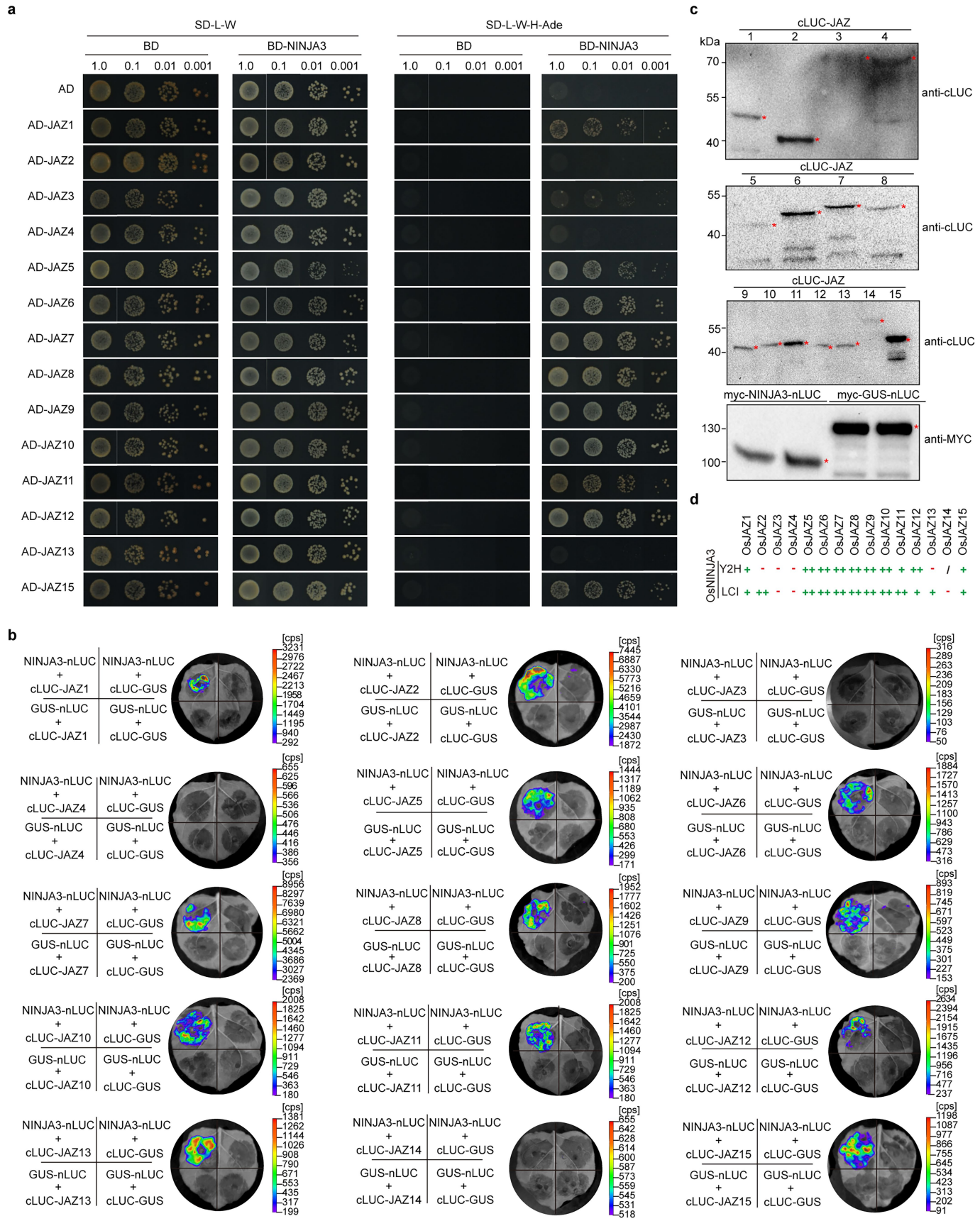

Extended Data Fig. 8 | NINJA3 interacts with most rice JAZ proteins to regulate JA signal transduction. a, Analysis of the interactions between OsJAZs and OsNINJA3 via Y2H assays. **b**, Analysis of the interactions between OsJAZs and OsNINJA3 via LCI assays. cps, signal counts per second. **c**, Protein detection of different transient expression combinations in the LCI assays **(b)**. The indicated proteins were detected via the corresponding antibodies. The red asterisks indicate the target protein bands. The analysis was repeated two to three times with similar results. **d**, Summary of the Y2H **(a)** and LCI **(b)** assays of the interaction between OsNINJA3 and OsJAZs. The strength of each interaction was rated as strong (++), weak (+) or undetectable (−).

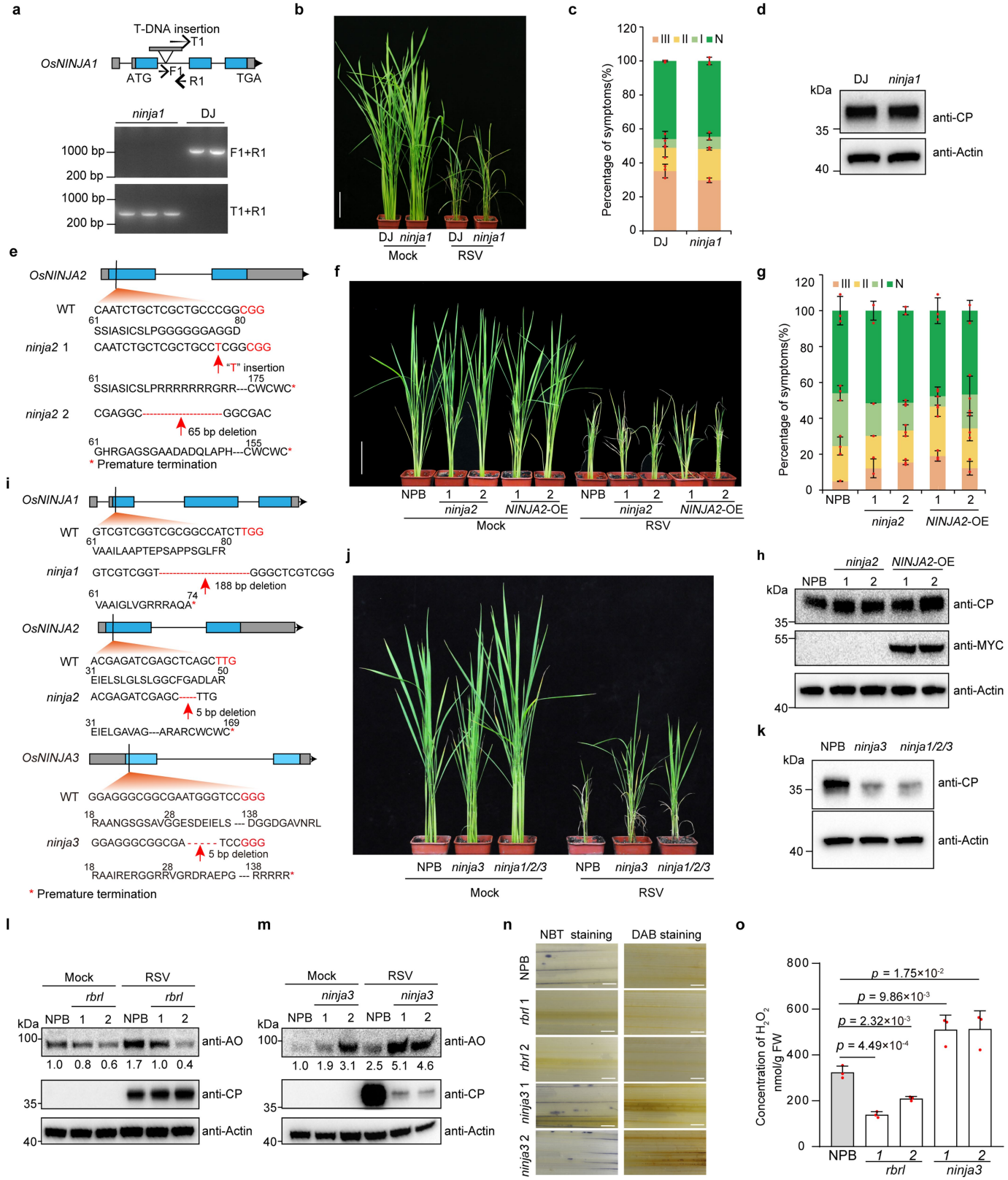

Extended Data Fig. 9 | See next page for caption.

Extended Data Fig. 9 | NINJA1 and NINJA2 are not involved in rice antiviral immunity, and the OsRBRL-OsNINJA3 module regulates the accumulation of downstream AO and ROS. a, Characterization of *ninja1* T-DNA insertion mutants. Schematic representation of the *OsNINJA1* gene and the position of the T-DNA insertion. F1, R1, and T1 represent the positions of the two primer pairs used to identify whether T-DNA insertion had occurred. **b**, Images showing mock-inoculated or RSV-infected Dongjing (DJ) and *ninja1* plants. Scale bar, 10 cm. **c**, Percentages of RSV-infected Dongjing (DJ) and *ninja1* plants with various disease symptom grades. The data are the mean ± s.d. $n = 3$ independent biological experiments. **d**, Immunoblotting analysis of the RSV CP levels in the specified plants. **e**, Generation of *ninja2*-knockout (CRISPR/Cas9) lines. The guide RNA (gRNA) sequence targeting *OsNINJA2* is indicated, and the protospacer-adjacent motif (PAM) is highlighted in red. In *ninja2* line 1, a 'T' insertion in the gRNA target site resulted in premature translational termination of *OsNINJA2*. In *ninja2* line 2, a 65-bp deletion in the gRNA target site resulted in premature termination of the translation of *OsNINJA2*. **f**, Images showing mock-inoculated or RSV-infected NPB, *ninja2* and *NINJA2*-OE plants. Scale bar, 10 cm. **g**, Percentages of RSV-infected NPB, *ninja2* and *NINJA2*-OE plants with various disease symptom grades. The data are the mean ± s.d. $n = 3$ independent biological experiments. **h**, Immunoblotting analysis of the RSV CP levels in the specified plants. **i**, Generation of *ninja1/2/3*-knockout (CRISPR/Cas9) lines. The guide RNA (gRNA) sequences targeting the indicated *OsNINJAs* are indicated, and the protospacer-adjacent motifs (PAMs) are highlighted in red. A 188-bp deletion in *NINJA1*, a 5-bp deletion in *NINJA2* and a 5-bp deletion in *NINJA3* resulted in premature translational termination of *OsNINJA1*, *OsNINJA2* and *OsNINJA3*. **j**, Images showing mock-inoculated or RSV-infected NPB, *ninja3* and *ninja1/2/3* plants. Scale bar, 10 cm. **k**, Immunoblotting analysis of the RSV CP levels in the specified plants. Rice plants were all collected at 4 w.p.i. **l**, Immunoblotting analysis of the AO levels in mock-inoculated and RSV-infected NPB and *rbrl* plants. **m**, Immunoblotting analysis of the AO levels in mock-inoculated and RSV-infected NPB and *ninja3* plants. Actin in **d**, **h**, **k**, **l**, and **m** served as sample processing controls. **n**, In situ detection of leaf ROS levels via DAB and NBT staining in the indicated rice plants. **o**, Quantification of H_2O_2 levels in the indicated rice plants. Statistical analysis was performed via two-sided Student's *t* tests, and all *p* values are shown in the figure. The data are the mean ± s.d. $n = 3$ independent biological samples. The analyses in **a**, **d**, **h**, and **k**-**n** were repeated two to three times with similar results.

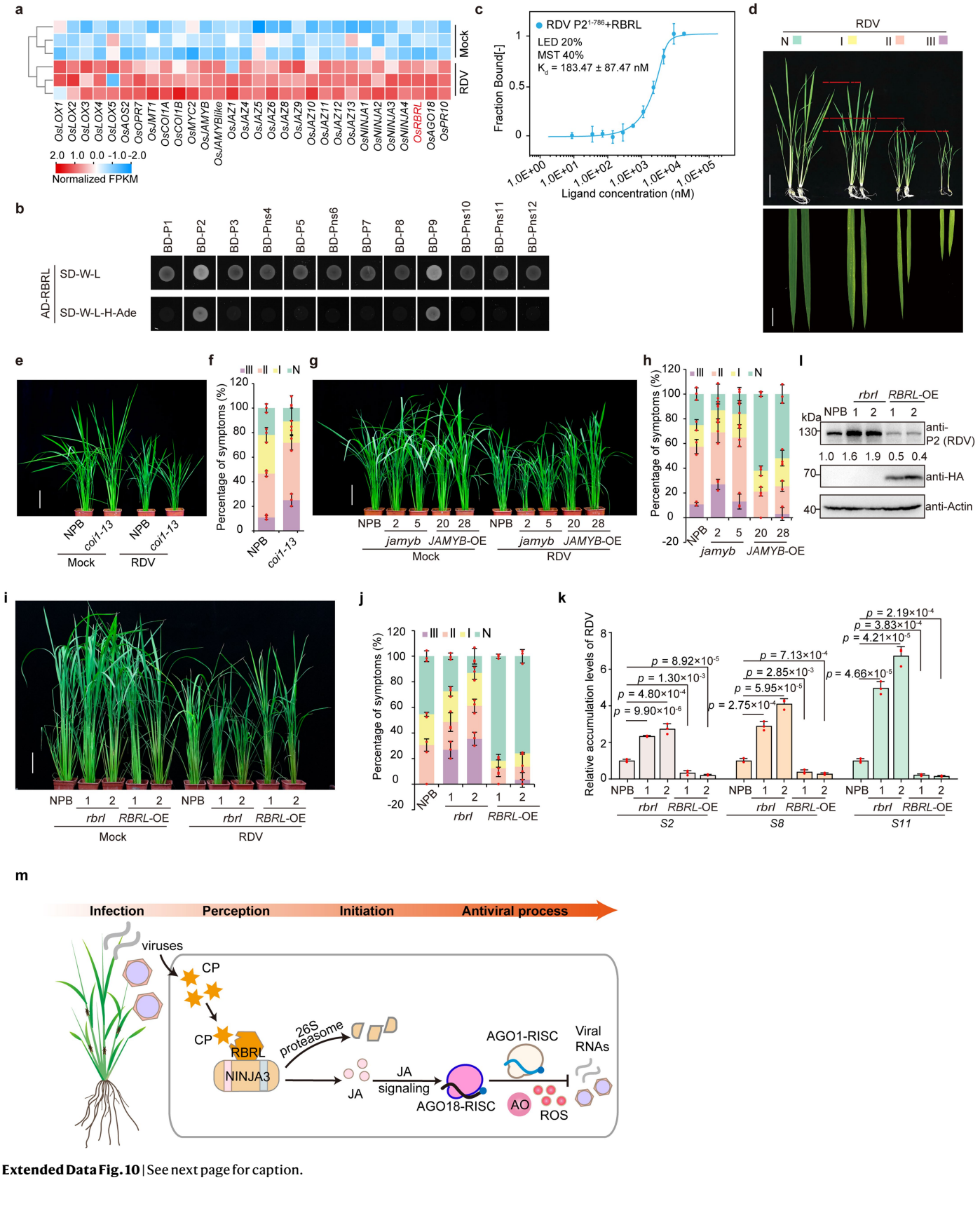

Extended Data Fig. 10 | See next page for caption.

Extended Data Fig. 10 | Jasmonate signalling mediates a broad-spectrum immune response against rice viruses. a, Expression analysis of genes related to JA synthesis and JA signalling in mock-inoculated and RDV-infected wild-type Zhonghua11 rice plants via transcriptome sequencing data from a previous study. The numbers are the Z scores of the FPKM values for each gene. FPKM, fragments per kilobase of transcript per million. **b**, Analysis of the interactions between RDV proteins and OsRBRL via Y2H assays. **c**, MST assays showing the binding affinity between RDV P2 N-terminus and OsRBRL. The data are the mean ± s.d. $n = 3$ independent biological samples. **d**, Photographs of RDV-infected NPB plants with different grades of disease symptoms. The photographs were taken at 4 w.p.i. Scale bars, 10 cm (upper panel) and 2 cm (bottom panel). N, no noticeable symptoms; I, typical yellow stripes on the leaves; II, typical yellow stripes on the leaves and mild chlorosis; III, typical yellow stripes on the leaves and severe chlorosis. From Grade N to Grade III, the dwarfism of the RDV-infected rice plants became increasingly severe. **e**, Images of mock-inoculated and RDV-infected NPB and *coi1-13* plants. Scale bar, 10 cm. **f**, Percentages of RDV-infected NPB and *coi1-13* plants with different disease symptom grades. The data are the mean ± s.d. $n = 3$ independent biological experiments. **g**, Images of mock-inoculated and RDV-infected NPB, *jamyb*, and *JAMYB*-OE plants. Scale bar, 10 cm. **h**, Percentages of RDV-infected NPB, *jamyb*, and *JAMYB*-OE plants with various disease symptom grades. The data are the mean ± s.d. $n = 3$ independent biological experiments. **i**, Images showing mock-inoculated and RDV-infected NPB, *rbrl*, and *RBRL*-OE plants. Scale bar, 10 cm. **j**, Percentages of RDV-infected NPB, *rbrl*, and *RBRL*-OE plants with various disease symptom grades. The data are the mean ± s.d. $n = 3$ independent biological experiments. **k**, RT–qPCR analysis of RDV RNA accumulation in the indicated plants. Statistical analysis was performed via two-sided Student's *t* tests, and all *p* values are shown in the figure. The data are the mean ± s.d. $n = 3$ independent biological samples. **l**, Immunoblotting analysis of RDV P2 levels in the indicated plants. OsRBRL expressed in *RBRL*-OE lines 1 and 2 was labelled with a 1× HA tag at the N-terminus. Actin served as loading controls. The analysis was repeated five times with similar results. **m**, A proposed working model for initiation of the antiviral immune response via RBRL. Rice plants were all collected at 4 w.p.i.

nature portfolio

Corresponding author(s): Li Yi

Last updated by author(s): Jan 17, 2025

Reporting Summary

Nature Portfolio wishes to improve the reproducibility of the work that we publish. This form provides structure for consistency and transparency in reporting. For further information on Nature Portfolio policies, see our Editorial Policies and the Editorial Policy Checklist.

Statistics

For all statistical analyses, confirm that the following items are present in the figure legend, table legend, main text, or Methods section.

n/a	Confirmed	
☐	☒	The exact sample size (*n*) for each experimental group/condition, given as a discrete number and unit of measurement
☐	☒	A statement on whether measurements were taken from distinct samples or whether the same sample was measured repeatedly
☐	☒	The statistical test(s) used AND whether they are one- or two-sided *Only common tests should be described solely by name; describe more complex techniques in the Methods section.*
☒	☐	A description of all covariates tested
☐	☒	A description of any assumptions or corrections, such as tests of normality and adjustment for multiple comparisons
☐	☒	A full description of the statistical parameters including central tendency (e.g. means) or other basic estimates (e.g. regression coefficient) AND variation (e.g. standard deviation) or associated estimates of uncertainty (e.g. confidence intervals)
☐	☒	For null hypothesis testing, the test statistic (e.g. *F*, *t*, *r*) with confidence intervals, effect sizes, degrees of freedom and *P* value noted *Give P values as exact values whenever suitable.*
☒	☐	For Bayesian analysis, information on the choice of priors and Markov chain Monte Carlo settings
☒	☐	For hierarchical and complex designs, identification of the appropriate level for tests and full reporting of outcomes
☒	☐	Estimates of effect sizes (e.g. Cohen's *d*, Pearson's *r*), indicating how they were calculated

Our web collection on statistics for biologists contains articles on many of the points above.

Software and code

Policy information about availability of computer code

Data collection	The fluorescence signal was detected using a confocal microscopy (LSM710, Zeiss). Images from immunoblotting were collected with Molecular Imager® ChemiDoc™M XRS+ (Bio-Rad). The luciferase activity was detected using a low-light cooled charge-coupled device imaging apparatus (NightOWL II LB983 with IndiGO software version 2.0.4.0). The luciferase activity was measured using a GLO-MAX 20/20 luminometer (Promega). Bio-Rad CFX96 with CFX Maestro 1.1 software was used in qRT-PCR analysis. For endogenous phytohormone quantification, JA analysis was performed on a mass spectrometer (UPLC 1290-MS/MS 6495). EASY-nLC 1200 liquid chromatography system and a C18 column coupled with a Thermo Fusion Lumos mass spectrometer were used to conduct IP-LC-MS/MS assays. The MST assays were performed on a Microscale Thermophoresis Monolith NT.115 instrument (NanoTemper Technologies, Munich, Germany). BioTek Cytation5 was used to quantify the H2O2 levels together with the Amplex Red Hydrogen Peroxide/Peroxidase Assay Kit.
Data analysis	Image analysis: ImageJ (version 1.45). Statistical analysis: GraphPad Prism (version 7.0). Phylogenetic tree: MEGA11. Conserved motif analysis: online MEME website (http://meme-suite.org/tools/meme). Raw sequence data quality control: FastQC software (version 0.12.0). The LC–MS/MS results were processed via Proteome Discoverer 2.2 software. MST data analyses were performed using the MO.Affinity analysis 3 software.

Sequence analysis: SnapGene (version 4.1.9).

For manuscripts utilizing custom algorithms or software that are central to the research but not yet described in published literature, software must be made available to editors and reviewers. We strongly encourage code deposition in a community repository (e.g. GitHub). See the Nature Portfolio guidelines for submitting code & software for further information.

Data

Policy information about availability of data

All manuscripts must include a data availability statement. This statement should provide the following information, where applicable:

- Accession codes, unique identifiers, or web links for publicly available datasets
- A description of any restrictions on data availability
- For clinical datasets or third party data, please ensure that the statement adheres to our policy

All source data associated with this work are available as part of the manuscript's supplementary information or as detailed below. OsRBRL (LOC_Os03g42760), OsRBRL-like (LOC_Os03g42780), OsNINJA1 (LOC_Os03g11550), OsNINJA2 (LOC_Os07g41160), OsNINJA3 (LOC_Os03g30570), OsNINJA4 (LOC_Os05g48500) are available from the Rice Genome Annotation Project Database (https://rice.uga.edu/). RNA-seq raw data have been deposited at the Genome Sequence Archive in National Genomics Data Center, China National Center for Bioinformation / Beijing Institute of Genomics, Chinese Academy of Sciences (GSA accession: CRA020855) that are publicly accessible at https://ngdc.cncb.ac.cn/gsa. Uncropped immunoblotting images are provided in Supplementary Fig. 1.

Research involving human participants, their data, or biological material

Policy information about studies with human participants or human data. See also policy information about sex, gender (identity/presentation), and sexual orientation and race, ethnicity and racism.

Reporting on sex and gender	NA
Reporting on race, ethnicity, or other socially relevant groupings	NA
Population characteristics	NA
Recruitment	NA
Ethics oversight	NA

Note that full information on the approval of the study protocol must also be provided in the manuscript.

Field-specific reporting

Please select the one below that is the best fit for your research. If you are not sure, read the appropriate sections before making your selection.

☒ Life sciences ☐ Behavioural & social sciences ☐ Ecological, evolutionary & environmental sciences

For a reference copy of the document with all sections, see nature.com/documents/nr-reporting-summary-flat.pdf

Life sciences study design

All studies must disclose on these points even when the disclosure is negative.

Sample size	The sample size and the results of statistical analyses are described in the relevant figures or method section. Sample size was determined based on experimental trials and previous publications on similar experiments (Yang et al., 2020, Cell Host & Microbe, 28, 89-103; Wang et al., 2020, Nature Communications, 11, 5830; Yao et al., 2022, Science Advances, 8, eabm0660; Yao et al., 2019, Molecular Plant, 12, 1114-1122; Wu et al., 2017, Nature Plants, 3, 16203; Wang et al., 2014, Nature Communications, 5, 4768).
Data exclusions	There is a pre-established criteria. For these experiments we always chose the plants in the same growth status to analysis infection rates, genes expressions, hormone contents and so on. Other plants will be excluded.
Replication	All experiments were repeated at least two or three times, and the number of independent experiments or biological replicates is indicated in the figure legends.
Randomization	All samples were arranged randomly into experimental groups. Plants for experiments were grown side by side to minimize unexpected environmental variations during growth.
Blinding	For different rice lines experiments, we firstly numbered these lines by one partner and the following analysis were done by other members to avoid subjective influence. For example, the virus-infection assay, different rice lines were numbered at first, the investigator was blinded to the group allocation during the experiments including the inoculation of viruliferous small brown planthopper, the infection rates statistics, and virus RNAs qRT-PCR analysis.

Reporting for specific materials, systems and methods

We require information from authors about some types of materials, experimental systems and methods used in many studies. Here, indicate whether each material, system or method listed is relevant to your study. If you are not sure if a list item applies to your research, read the appropriate section before selecting a response.

Materials & experimental systems

n/a	Involved in the study
[ ]	[x] Antibodies
[x]	[ ] Eukaryotic cell lines
[x]	[ ] Palaeontology and archaeology
[x]	[ ] Animals and other organisms
[x]	[ ] Clinical data
[x]	[ ] Dual use research of concern
[ ]	[x] Plants

Methods

n/a	Involved in the study
[x]	[ ] ChIP-seq
[x]	[ ] Flow cytometry
[x]	[ ] MRI-based neuroimaging

Antibodies

Antibodies used

anti-CM-LOX2 (custom-developed by ABclonal® Technology, China, generated in Yang et al., 2020, Cell Host & Microbe, DOI: 10.1016/j.chom.2020.05.001, and was preserved by our laboratory);
anti-AOS2 (custom-developed by ABclonal® Technology, China, generated in Yang et al., 2020, Cell Host & Microbe, DOI: 10.1016/j.chom.2020.05.001, and was preserved by our laboratory);
anti-RSV CP (provided by Dr. Jianxiang Wu from Zhejiang University, generated in Fu et al., 2018, Molecular Plant, DOI: 10.1016/j.molp.2017.11.011);
anti-RDV P2 (custom-developed by ABclonal® Technology, China, generated in Jin et al., 2016, PLoS Pathogens, DOI: 10.1371/journal.ppat.1005847, and was preserved by our laboratory);
anti-AGO18 (custom-developed by ABclonal® Technology, China, generated in Wu et al., 2015, eLife, DOI: 10.7554/eLife.05733, and was preserved by our laboratory);
anti-AO (custom-developed by Integrated R&D Services- WuXi AppTec, generated in Wu et al., 2017, Nature Plants, DOI: 10.1038/nplants.6 2016.203, and was preserved by our laboratory);
anti-RBRL (custom-developed by ABclonal® Technology, China, generated in this study);
anti-NINJA3 (custom-developed by ABclonal® Technology, China, generated in this study);
anti-MYC (ABclonal, Wuhan, China, Cat#AE010);
anti-HA (ABclonal, Wuhan, China, Cat#AE008);
anti-GFP/YFP (ABclonal, Wuhan, China, Cat#AE012);
anti-GST (ABclonal, Wuhan, China, Cat#AE001);
anti-MBP (ABclonal, Wuhan, China, Cat#AE016);
anti-FLAG (TransGen Biotech, Beijing, China, Cat#HT201);
anti-S (EarthOx, Cat#E022130);
anti-OsFBPA (Beijing Protein Innovation, Beijing, China, Cat#AbP80247-A-SE);
anti-Histone H3 (Abcam, Cat#ab1791);
anti-cLUC (Sigma-Aldrich, America, Cat#L2164);
anti-Actin (CWBIO, Beijing, China, Cat#CW0096M);
anti-PAG1 (generated in Han et al., 2019, New Phytologist, DOI:10.1111/nph.15471, and was preserved by our laboratory).

Validation

Validation statements and experiments can be obtained from the following websites and publications:
Anti-CM-LOX2 (DOI: 10.1016/j.chom.2020.05.001), species: Oryza sativa subsp. japonica, application: immunoblotting;
anti-AOS2 (DOI: 10.1016/j.chom.2020.05.;01), species: Oryza sativa subsp. japonica, application: immunoblotting;
anti-RSV CP (DOI: 10.1016/j.chom.2020.05.001), species: Rice stripe virus, application: immunoblotting and immunoprecipitation;
anti-RDV P2 (DOI: 10.1093/mp/ssu007), species: Rice dwarf virus, application: immunoblotting;
anti-AGO18 (DOI: 10.7554/eLife.05733), species: Oryza sativa subsp. japonica, application: immunoblotting;
anti-AO (DOI: 10.1038/nplants.6 2016.203), species: Oryza sativa subsp. japonica, application: immunoblotting;
anti-RBRL (generated in this study), species: Oryza sativa subsp. japonica, application: immunoblotting;
anti-NINJA3 (generated in this study), species: Oryza sativa subsp. japonica, application: immunoblotting;
anti-MYC (https://abclonal.com.cn/catalog/AE010), application: immunoblotting;
anti-HA (https://abclonal.com.cn/catalog/AE008), application: immunoblotting;
anti-GFP/YFP (https://abclonal.com.cn/catalog/AE012), application: immunoblotting;
anti-GST (https://abclonal.com.cn/catalog/AE001), application: immunoblotting;
anti-MBP (https://abclonal.com.cn/catalog/AE016), application: immunoblotting;
anti-FLAG (https://www.transgen.com/antibody_tag/371.html), application: immunoblotting;
anti-S (EarthOx, Cat#E022130, https://earthox.net/product-category/life-science-products/antibodies/), application: immunoblotting;
anti-OsFBPA (http://www.proteomics.org.cn/product/818.html), species: Oryza sativa subsp. japonica, application: immunoblotting;
anti-Histone H3 (https://www.abcam.cn/products/primary-antibodies/histone-h3-antibody-nuclear-marker-and-chip-grade-ab1791.html), species: Oryza sativa subsp. japonica, application: immunoblotting;
anti-cLUC (https://www.sigmaaldrich.cn/CN/zh/product/sigma/l2164), application: immunoblotting;
anti-Actin (https://www.cwbio.com/goods/index/id/10113), species: Oryza sativa subsp. japonica and Nicotiana benthamiana, application: immunoblotting.
anti-PAG1 (DOI:10.1111/nph.15471), species: Oryza sativa subsp. japonica and Arabidopsis thaliana, application: immunoblotting.

Dual use research of concern

Policy information about dual use research of concern

Hazards

Could the accidental, deliberate or reckless misuse of agents or technologies generated in the work, or the application of information presented in the manuscript, pose a threat to:

No	Yes	
☒	☐	Public health
☒	☐	National security
☒	☐	Crops and/or livestock
☒	☐	Ecosystems
☒	☐	Any other significant area

Experiments of concern

Does the work involve any of these experiments of concern:

No	Yes	
☒	☐	Demonstrate how to render a vaccine ineffective
☒	☐	Confer resistance to therapeutically useful antibiotics or antiviral agents
☒	☐	Enhance the virulence of a pathogen or render a nonpathogen virulent
☒	☐	Increase transmissibility of a pathogen
☒	☐	Alter the host range of a pathogen
☒	☐	Enable evasion of diagnostic/detection modalities
☒	☐	Enable the weaponization of a biological agent or toxin
☒	☐	Any other potentially harmful combination of experiments and agents

Plants

Seed stocks	The wild-type NPB were preserved by our laboratory. The wild-type DJ was provided by Dr. Lizhong Xiong from the National Key Laboratory of Crop Genetic Improvement, Hubei Hongshan Laboratory, Huazhong Agricultural University.
Novel plant genotypes	The overexpression rice lines of OsRBRL, RSV CP, OsNINJA2 and OsNINJA3 were generated through transgenic methods. The knockout rice lines of OsRBRL, OsNINJA1, OsNINJA2 and OsNINJA3 were generated using CRISPR/Cas9.
Authentication	The coi1-13 mutant was identified through qRT–PCR and phenotypic observation, which is consistent with prior reports. The jamyb mutant was identified by sequencing, as previously described. The ninja1 (modd-2) mutant was identified by genotyping using gene-specific and T-DNA-specific primers as described previously.The rice lines overexpressing OsRBRL, RSV CP, and OsNINJA3 were verified by immunoblotting. The genome-edited mutants were confirmed by sequencing and analyzed using SnapGene (https://www.snapgene.com).